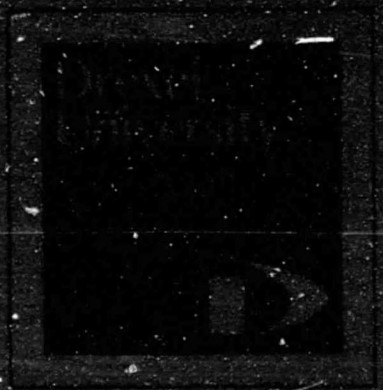

A SINGULAR PERTURBATION ANALYSIS OF MINIMUM TIME LONG RANGE INTERCEPT

Final Report
January, 1980

Research Supported by N.A.S.A. Langley Research Center
NASA Grant No. NSG-1496
Principal Investigator: Dr. Anthony J. Calise
Research Assistant: Mr. Daniel D. Moerder

MECHANICAL ENGINEERING AND MECHANICS DEPARTMENT
DREXEL UNIVERSITY
PHILADELPHIA, PENNSYLVANIA 19104

TABLE OF CONTENTS

LIST OF FIGURES

LIST OF FIGURES

1. INTRODUCTION

This report gives a brief summary of the research accomplished under this grant and a more detailed report on the activities during the last reporting period, from July, 1979 to January, 1980. The major objective of this research was to explore the application of singular perturbation theory for deriving algorithms suitable for on-board, real-time computation of optimal aircraft trajectory control. Minimum time intercept in three dimensions was selected as a pilot problem formulation, and data for an early version F-4 aircraft was used to represent aircraft aerodynamic and propulsion characteristics. The major products of this research are the derivation of nonlinear, near-optimal feedback control laws that are readily implementable in an aircraft flight computer, performance results for a variety of initial conditions (including optimal intercept at short ranges), and a point-mass three dimensional simulation suitable for representing fighter aircraft under closed-loop optimal control. A new grant has been initiated to utilize the results of this research first in a piloted simulation at NASA Langley and later in an actual flight test at the NASA Dryden research center.

2. SUMMARY OF RESULTS FOR 1978

The details of the research accomplished during the first 18 months are documented in References [1] - [3]. At this stage it was felt that a major milestone had been reached and the results were published in [4]. Reference [1] presents the problem formulation and singular perturbation analysis of the position, energy and heading dynamics. Altitude and flight path angle dynamics were not optimized. Reference [2] demonstrates the feasibility of on-board computation of the optimal control solution. During this period

the optimal control solution was implemented in a feedback form as a control subroutine in a computer simulation of the F-4 aircraft. Since the altitude and flight path angle dynamics were not optimized, a simple proportional controller was used to calculate the required lift in the vertical plane based on the optimal altitude derived from optimization of the instantaneous energy, heading and relative position dynamics. Performance results were obtained for a variety of intercept conditions and an estimate was obtained of the CPU time and storage requirements for the control algorithm. In addition, the analysis was extended to the case of intercept at short ranges. This exhibits solutions that do not contain a constant altitude cruise leg.

3. SUMMARY OF RESULTS FOR 1979

The research this past year has been concentrated in four main areas:

1. Optimization of altitude and flight path angle dynamics
2. Optimization for the short range case
3. Implementation and evaluation of a proportional-plus-integral (P-I) controller for vertical lift calculation when altitude and flight path angle dynamics are not optimized.
4. Off-line, open loop optimization using a conjugate gradient numerical optimization program.

This section will detail the analysis for optimization of altitude and flight path angle dynamics and then conclude with example numerical results for the four areas cited above.

3.1 Optimization of Altitude and Flight Path Angle Dynamics

The analysis in this section assumes familiarity with the analysis in [1] and [2]. The same notation is continued here. At this point the performance

index was generalized from minimum time to include a term penalizing large flight path angles

$$J = \int 1 + k \sin^2 \gamma \, d\gamma \tag{1}$$

and in addition a constraint was imposed on the maximum value for γ

$$|\gamma| \leq \gamma_{max} < \pi/2 \tag{2}$$

The above modifications to the problem formulation do not alter the analysis in [1] and [2].

Third Boundary Layer

The Hamiltonian in the third (altitude) boundary layer is:

$$L_1 = W \cos \gamma \tag{3}$$

$$H_3 = H_1 (h,E,\beta,\gamma) - \lambda_{E_1} L_n^2 KV/qsW + \lambda_{\beta_2} L_n g/WV \cos \gamma + \lambda_h V \sin \gamma$$

$$+ \nu_1 (\gamma_{max}^2 - \gamma^2) + \nu_2 \{L_{max}^2 - W^2 \cos^2 \gamma - L_n^2\} = 0 \tag{4}$$

where H_1 is the first boundary layer Hamiltonian evaluated at present values of altitude (h), energy (E), heading (β) and flight path angle

$$H_1 = (\lambda_{x_o} \cos \beta + \lambda_{y_o} \sin \beta) V \cos \gamma - \lambda_{y_o} V_T \cos \gamma_T$$

$$+ \gamma_{E_1} (T - D_o) V/W + 1 + k \sin^2 \gamma \tag{5}$$

and

$$D_o = q_s C_{D_o} + KW^2 \cos^2 \gamma / qs \tag{6}$$

The parameters λ_{x_o}, λ_{y_o}, λ_{E_1} and λ_{β_2} are known from previous outer and boundary layer solutions. The controls are γ and the horizontal component of lift (L_n).

So we have

$$\partial H_3/\partial \gamma = 0 \tag{7}$$

$$\partial H_3/\partial L_n = 2\lambda_{E_1} L_n KV/qsW + \lambda_{\beta_2} g/WV \cos \gamma - 2\nu_2 L_n = 0 \tag{8}$$

Note that $\nu = 0$ off the constraint bound and L_n can be determined as a function of γ from (7). On the constraint bound $L_n^2 = L_{max}^2 - W^2 \cos^2 \gamma$ and ν can be determined as a function of γ. In either case, L_n and ν can be regarded as functions of γ and other known parameters. Hence, we need only combine (7) with (4) to compute the optimum flight path angle (γ_3) and corresponding costate (λ_{γ_3}). To do this we follow the procedure used in the first and second boundary layer and write

$$\gamma_3 = \arg \{\max_{\gamma} [\frac{\sin \gamma}{H_2(h,E,\beta,\gamma)}] \} \cdot \text{sign} \{h_2 - h\} \tag{9}$$

where H_2 is the second boundary layer Hamiltonian

$$H_2 = H_1 - \lambda_{E_1} L_n^2 KV/qsW + \lambda_{\beta_2} L_n g/WV \cos \gamma \tag{10}$$

The maximization in (9) is performed over the range $0 \leq \gamma \leq \gamma_{max}$, where we have used the fact that sign $\{\lambda_h\}$ = - sign $\{\gamma\}$ = sign $\{h - h_2\}$ and h_2 is the optimum altitude from the second boundary layer. Since it is possible for H_2 to change sign it was decided to instead use the form

$$\gamma_3 = \arg \{\min_{\gamma} [H_2/\sin \gamma]\} \cdot \text{sign} \{h_2 - h\} \tag{11}$$

Having determined γ_3 and L_{n_3}, λ_{h_3} can be computed using (4)

$$\lambda_{h_3} = -[H_1 - \lambda_{E_1} L_{n_3}^2 KV/qsW + \lambda_{\beta_2} L_{n_3} g/WV \cos \gamma_3]/V \sin \gamma \tag{12}$$

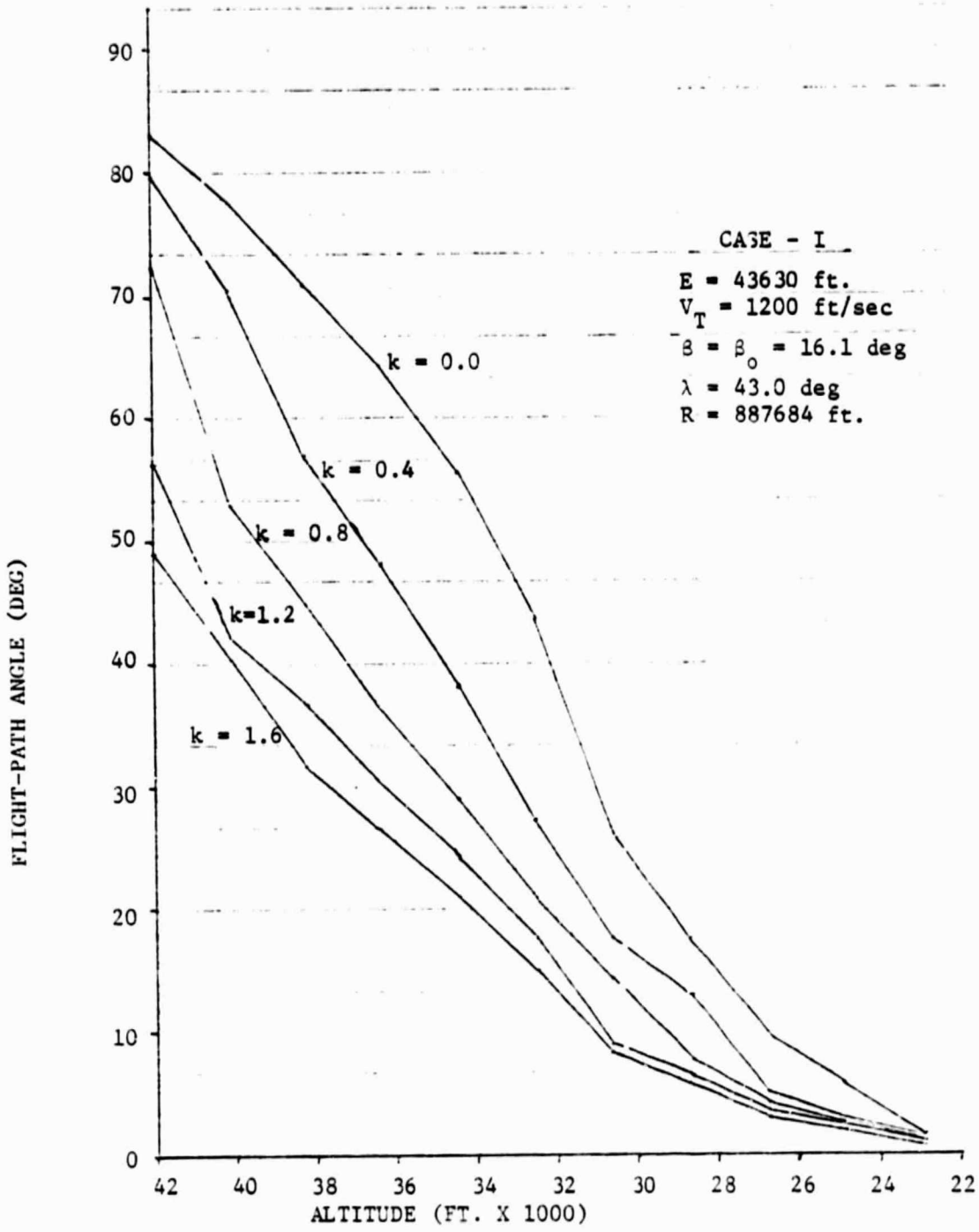

FIGURE 1. OPTIMUM FLIGHT-PATH ANGLE FROM THIRD BOUNDARY LAYER ANALYSIS

Numerical results for γ_3 as a function of the altitude error for a zero and non-zero heading errors are shown in Fig. 1. The effect of the weighting parameter (k) in the performance index (1) is also shown.

Fourth Boundary Layer

For solutions off the lift constraint bound we write the fourth boundary layer Hamiltonian in the form

$$H_4 = H_3(h,E,\beta,\gamma) - \lambda_{E_1} K(2\delta L_1 W \cos\gamma + \delta L_1^2 + 2(\delta L_n L_{n_3} + \delta L_n^2)V/qsW, + \lambda_{\beta_2}\delta L_n g/WV \cos\gamma + \lambda_\gamma \delta L_1 g/WV = 0 \quad (13)$$

where δL_1 and δL_n are perturbations in the controls from the third boundary layer solutions.

$$\delta L_1 = L_1 - W\cos\gamma \quad (14)$$

$$\delta L_n = L_n - L_{n_3} \quad (15)$$

Using the conditions $H_4 = 0$, $\partial H_4/\partial \delta L_1 = 0$ and $\partial H_4/\partial \delta L_n = 0$ we obtain the following solutions:

$$\delta L_{n_4} = \lambda_{\beta_2} qgs/2\lambda_{E_1} KV^2 \cos\gamma - L_{n_3} \quad (16)$$

$$\delta L_{14} = [-H_3 qsW/\lambda_{E_1} KV - \delta L_{n_4}^2]^{1/2} \cdot \text{sign}\,(\gamma_3 - \gamma) \quad (17)$$

The final lift and bank angle equations are

$$L = [(W\cos\gamma + \delta L_{14})^2 + L_{n_4}^2]^{1/2} \quad (18)$$

$$\mu = \tan^{-1}(L_{n_4}/L_{14}) \quad (19)$$

If L in (18) exceeds L_{max} then we set $L = L_{max}$ and reformulate the necessary conditions to find the optimum bank angle. Letting

$$L_1 = L_{max} \cos \mu \tag{20}$$

$$L_n = L_{max} \sin \mu \tag{21}$$

Then from $\partial H_4/\partial \mu = 0$ we obtain

$$\tan \mu = (\lambda_{\beta_2}/\lambda_\gamma \cos \gamma) \cdot \text{sign } (\phi_o - \phi) \tag{22}$$

Using (22) in $H_4 = 0$ we can evaluate λ_γ as one of the roots of

$$A\lambda_\gamma^2 + B\lambda_\gamma + C = 0 \tag{23}$$

where

$$A = g^2[L_{max}^2/W^2 - \cos^2 \gamma]/V^2 \tag{24}$$

$$B = 2\Phi \cos \gamma g/V \tag{25}$$

$$C = (\lambda_{\beta_2} L_{max} g/WV \cos \gamma)^2 - \Phi^2 \tag{26}$$

and

$$\Phi = H_1 - \lambda_{E_1}(L_{max}^2 - W^2\cos^2\gamma)\, KV/qsW + \lambda_{h_3} V \sin \gamma \tag{27}$$

In Appendix A it is shown that (23) will always have real roots with opposite sign. So the root of (23) is chosen such that

$$\text{sign } \{\lambda_\gamma\} = -\text{sign } \{\gamma_3 - \gamma\} \tag{28}$$

With this value of λ_γ the optimum bank angle is computed using (22), taking care to place μ in the proper quadrant based also on the sign of $\{\gamma_3 - \gamma\}$

3.2 Numerical Results

This section documents the results of numerical tests made to verify the analytical results in this report. The aircraft simulation model used in this study is the same as in [2]. The optimal control computation requirements, including the third and fourth boundary layer optimization, were 0.07 seconds for update and 50198 bytes of core space versus 0.03 seconds per update and 43724 bytes for the suboptimal control described in [2]. The increase in computation time is primarily due to the third boundary layer computation, which requires a numerical search over (11).

Two test cases were investigated in the development of the fully optimized control. The first test case in Case I from [2] starting at t = 87 seconds, at which point heading error is near zero, with the aircraft moved to an altitude of 40,000 feet while holding total initial energy constant, thus introducing a large initial altitude error. This case is hereafter referred to as Case I-A. The second test case examined is Case III in [2]. Case III was chosen for the hard initial turn required of the aircraft for intercept, which resulted in a commanded altitude above the climb path. The aircraft in this case is initially close to the zero-heading-error optimum climb path. The initial geometries in the horizontal plane are displayed in Fig. 2. The trajectories were stopped at 200 seconds for Case I-A and at 60 seconds for Case III, displaying initial transient phases only. This is sufficient to show the effect of the third and fourth boundary layer optimization since the control solution converges to the second boundary layer solution as the flight path angle and altitude errors approach zero. Figures 3 through 15 display actual and commanded flight path angle and altitude histories and lift and bank angle histories for Cases I-A and III and altitude versus mach number plots for Case III, both with fully optimized control. and with proportional vertical lift control as in [2].

In Case I-A the control failed twice due to numerical difficulties encountered when the altitude error became small. This can be seen in Fig. 7 where the commanded flight path angle (GMD) discontinuously jumps to its constrained maximum at approximately 90 and 160 seconds. Note the altitude errors in Fig. 4 at these times. The computer implementation of the control algorithm called for this when the first bracketed term of (11) became negative. The numerical problem leading to the excursions can be traced to the fact that both the numerator and denominator in (11) asymptotically approach zero as the aircraft altitude approaches the second boundary layer commanded altitude (the optimal flight path angle also approaches zero under these circumstances). It should be noted that the calculation of λ_{β_2} in [2] takes the form:

$$\lambda_{\beta_2} = (\lambda_{E_1} V_2 KL_n^2/qsW - H_1)\ mV_2/L_n \tag{29}$$

and is prone to considerable inaccuracy when the heading error is very small, since L_n approaches 0. Doubtless, the carryover of second boundary layer inaccuracies into the third aggravated the numerical difficulties. It can be shown, however, employing l'Hospital's rule, that (11) does in fact converge to zero. With this encouragement, modifications are currently being made to the algorithm to circumvent these problems.

No discontinuities are seen in the Case III trajectory (Figs. 9, 11, 13) since the third boundary layer control solution had not converged to that of the second at any point. It is of interest in this case to note the appreciable difference between the altitude versus mach plots for proportional and fully optimized control, seen in Figs. 14 and 15.

Although no test trajectories were run fully to intercept, it is estimated, based on use of the tabular first boundary layer data in [2] over straight-line approximations for the intercept paths, that the time savings accrued in both

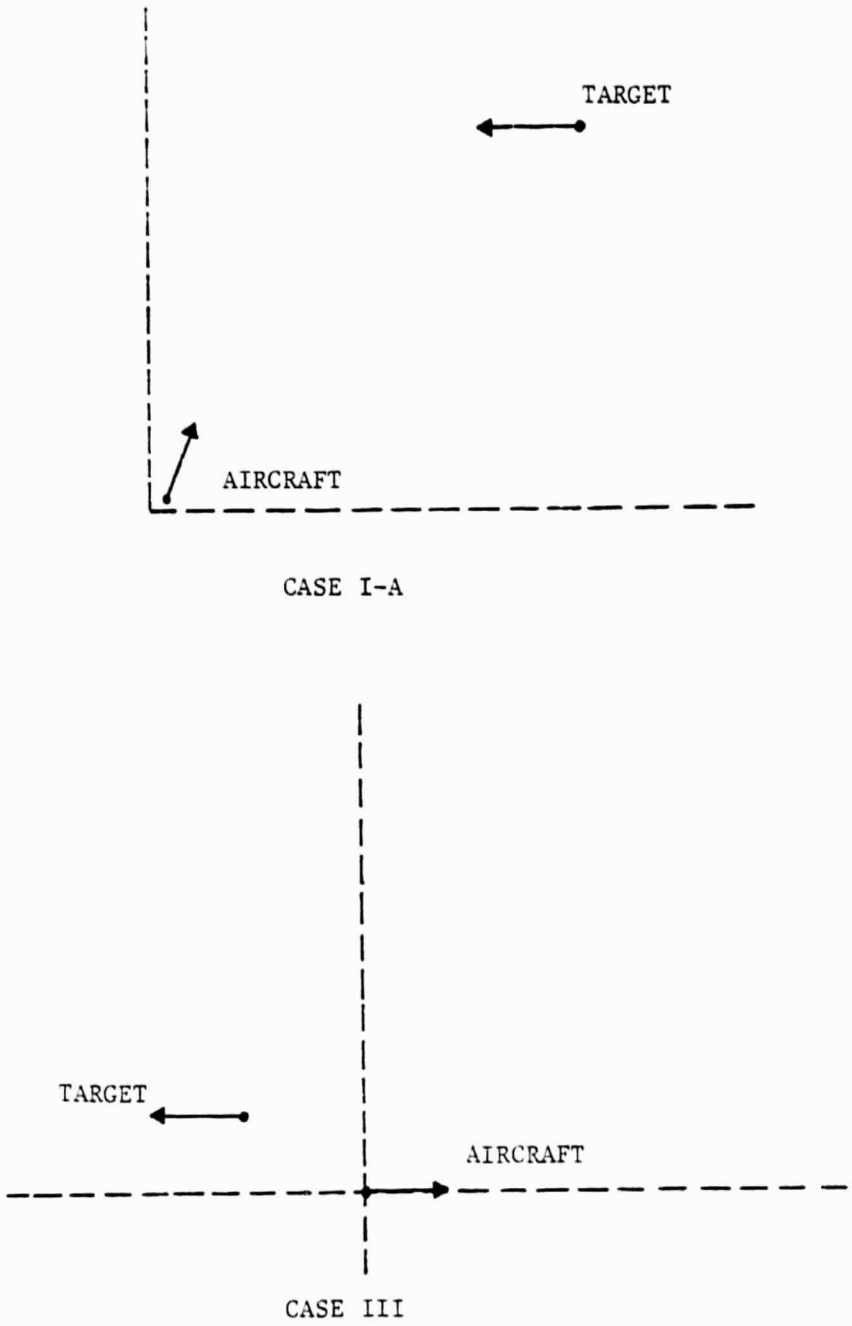

FIGURE 2. HORIZONTAL PLANE PROJECTIONS OF INITIAL GEOMETRIES FOR CASES TREATED IN STUDY

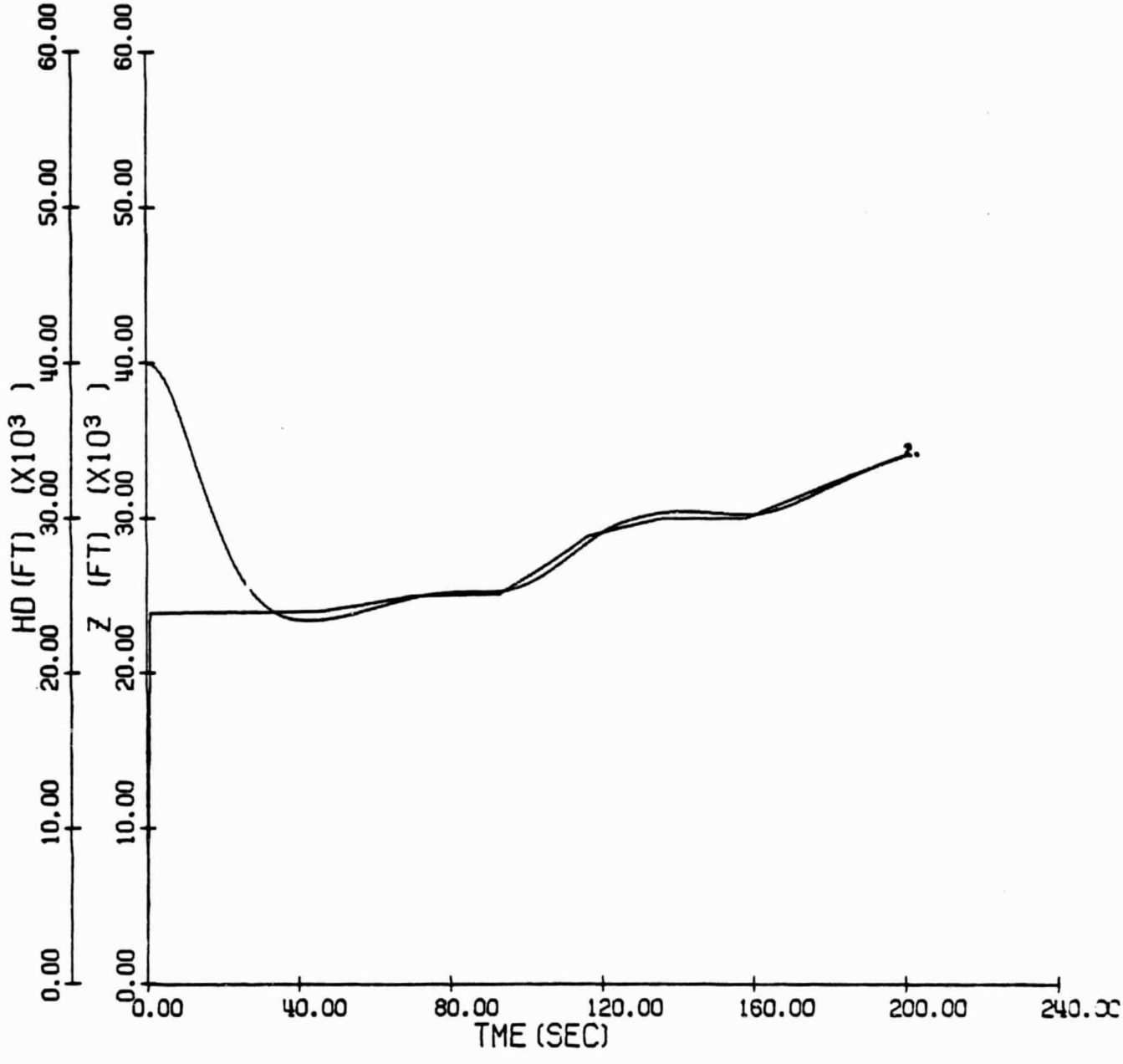

FIGURE 3. ACTUAL AND COMMANDED ALTITUDE FOR CASE I-A WITH PROPORTIONAL SUBOPTIMAL CONTROL

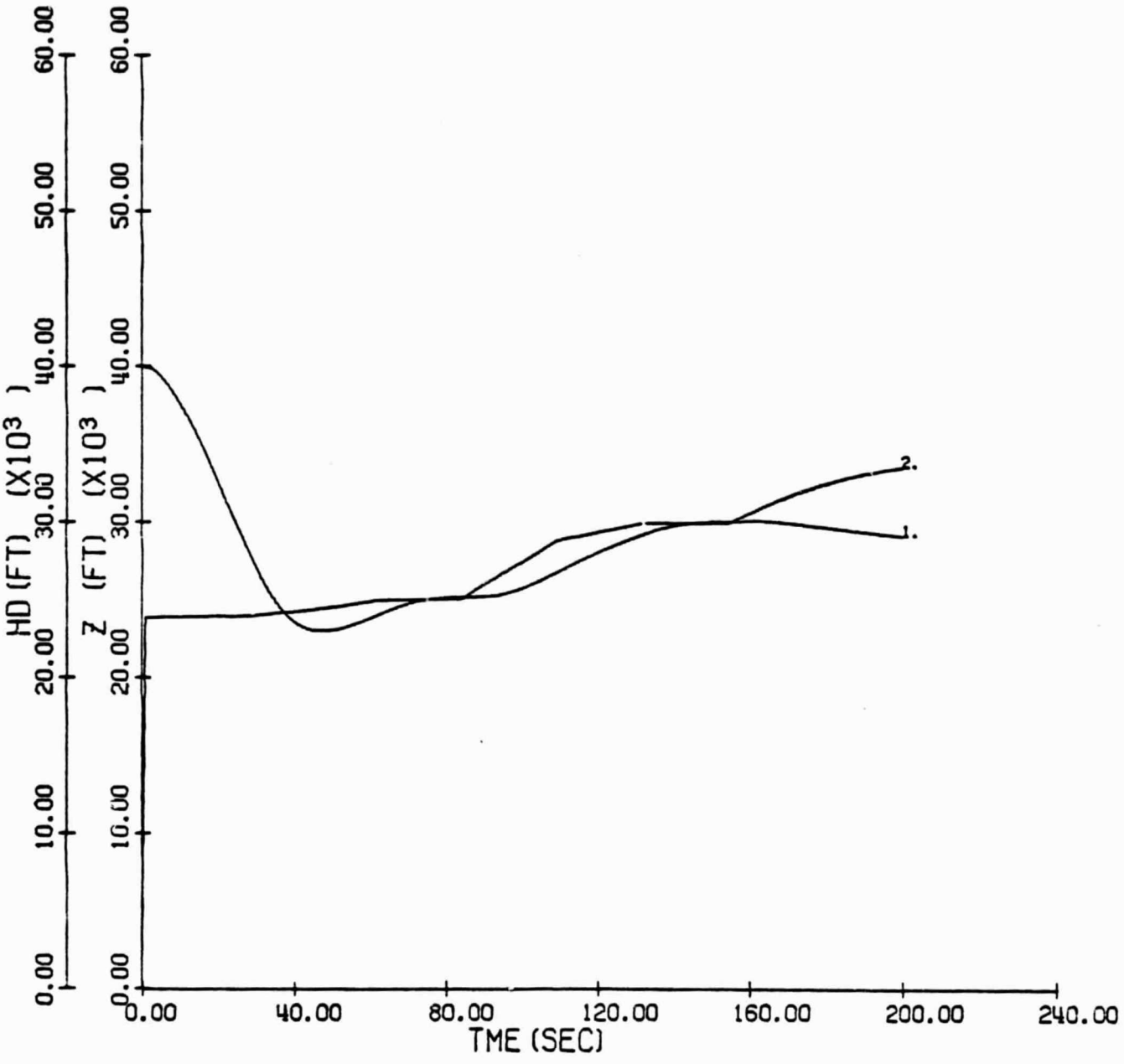

FIGURE 4. ACTUAL AND COMMANDED ALTITUDE FOR CASE I-A WITH FULLY OPTIMIZED LIFT AND BANK ANGLE

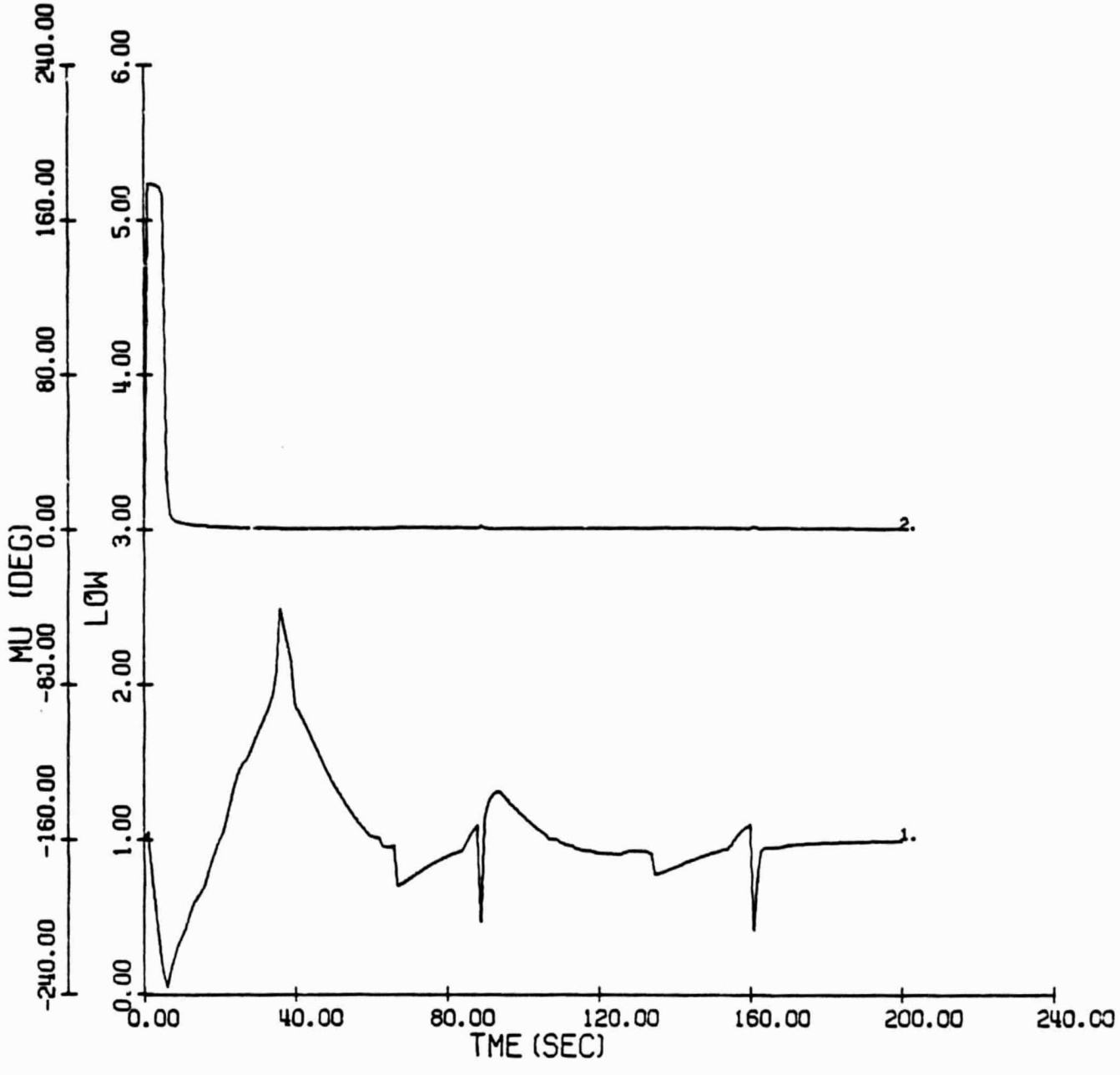

FIGURE 5. LIFT AND BANK ANGLE FOR CASE I-A WITH FULLY OPTIMIZED LIFT AND BANK ANGLE

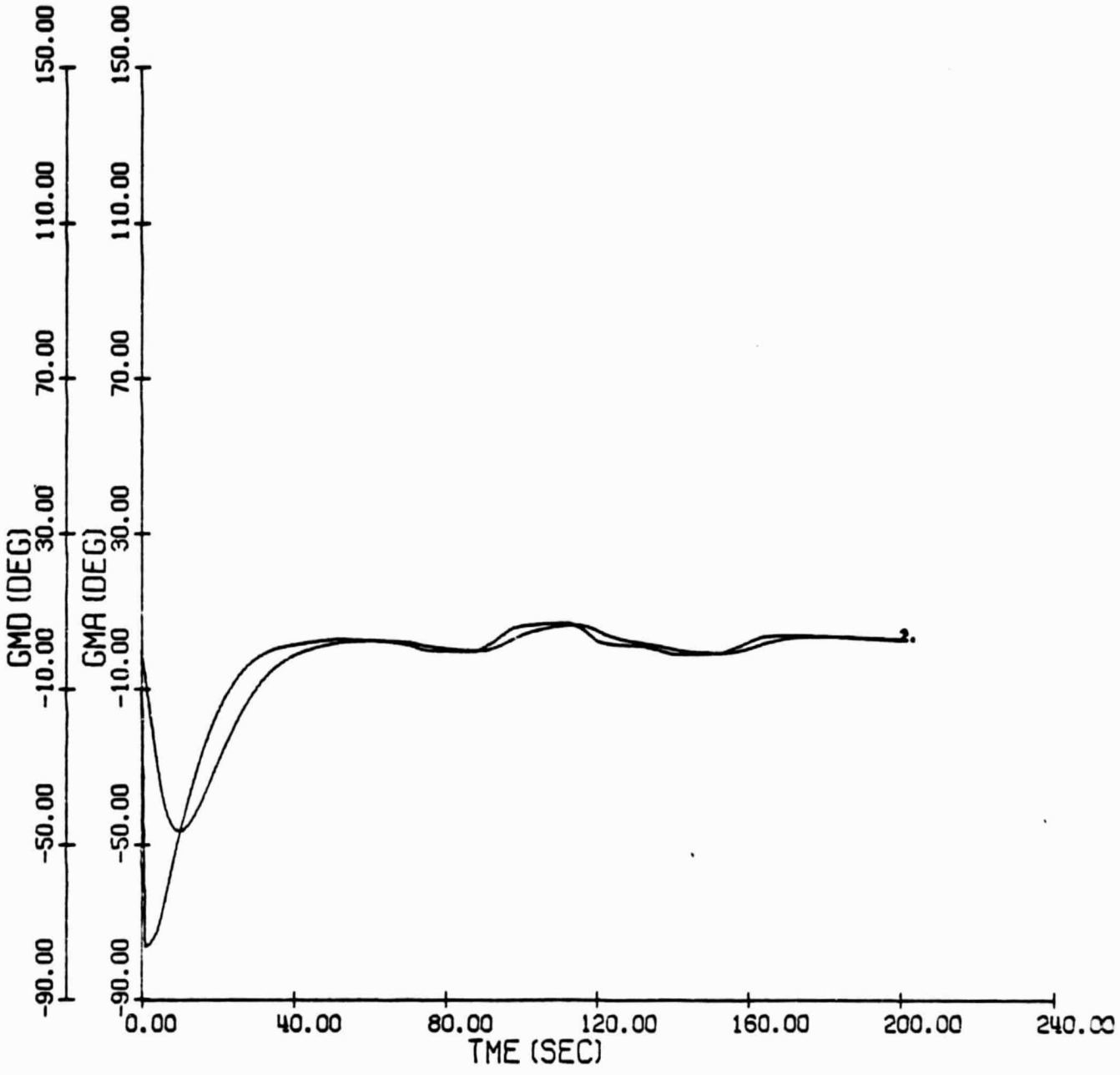

FIGURE 6. ACTUAL AND COMMANDED FLIGHT PATH ANGLE FOR CASE I-A WITH SUBOPTIMAL PROPORTIONAL CONTROL

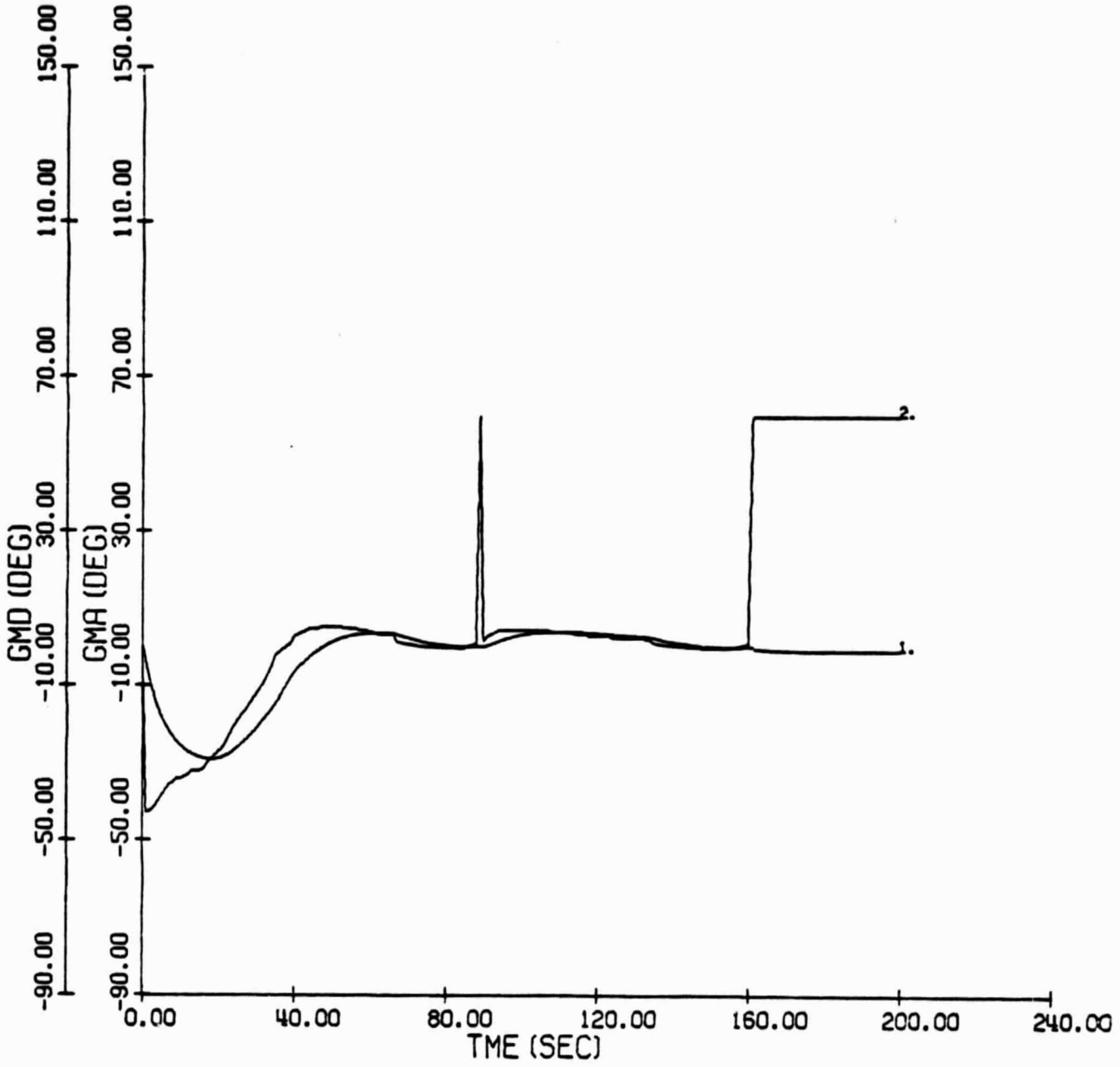

FIGURE 7. ACTUAL AND COMMANDED FLIGHT PATH ANGLE FOR CASE I-A WITH FULLY OPTIMIZED LIFT AND BANK ANGLE.

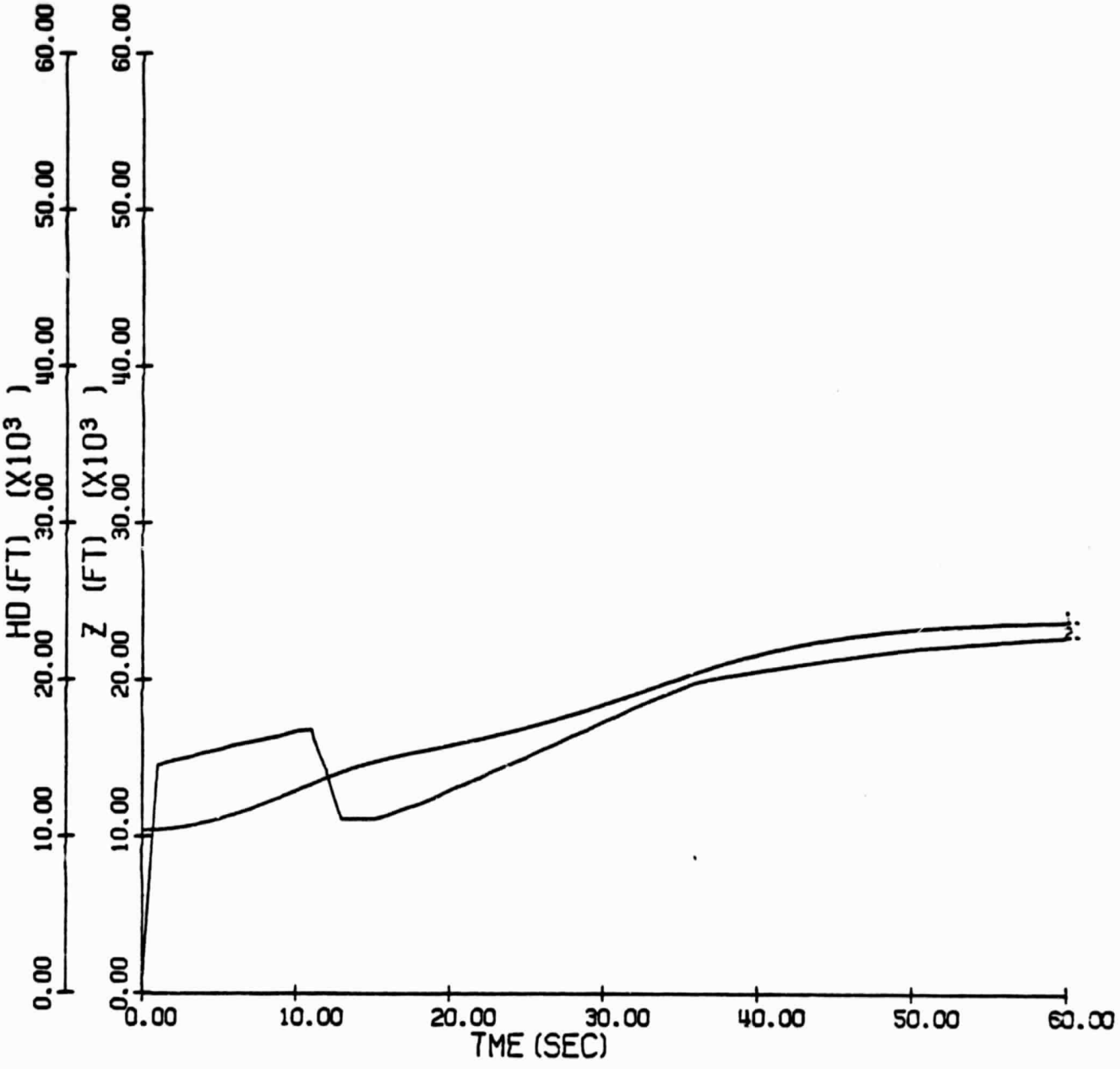

FIGURE 8. ACTUAL AND COMMANDED ALTITUDE FOR CASE III WITH PROPORTIONAL SUBOPTIMAL CONTROL

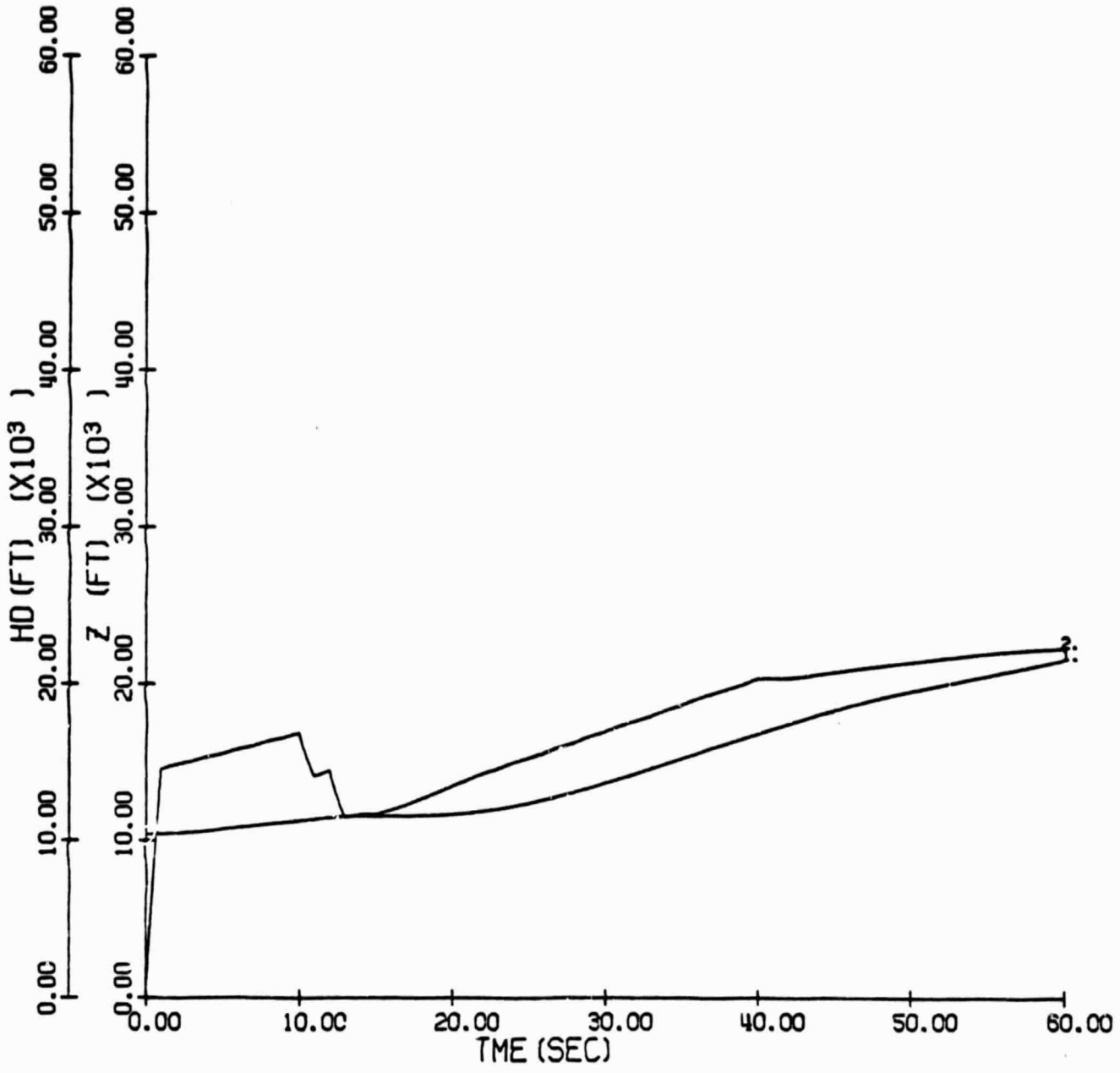

FIGURE 9. ACTUAL AND COMMANDED ALTITUDE FOR CASE III WITH FULLY OPTIMIZED LIFT AND BANK ANGLE

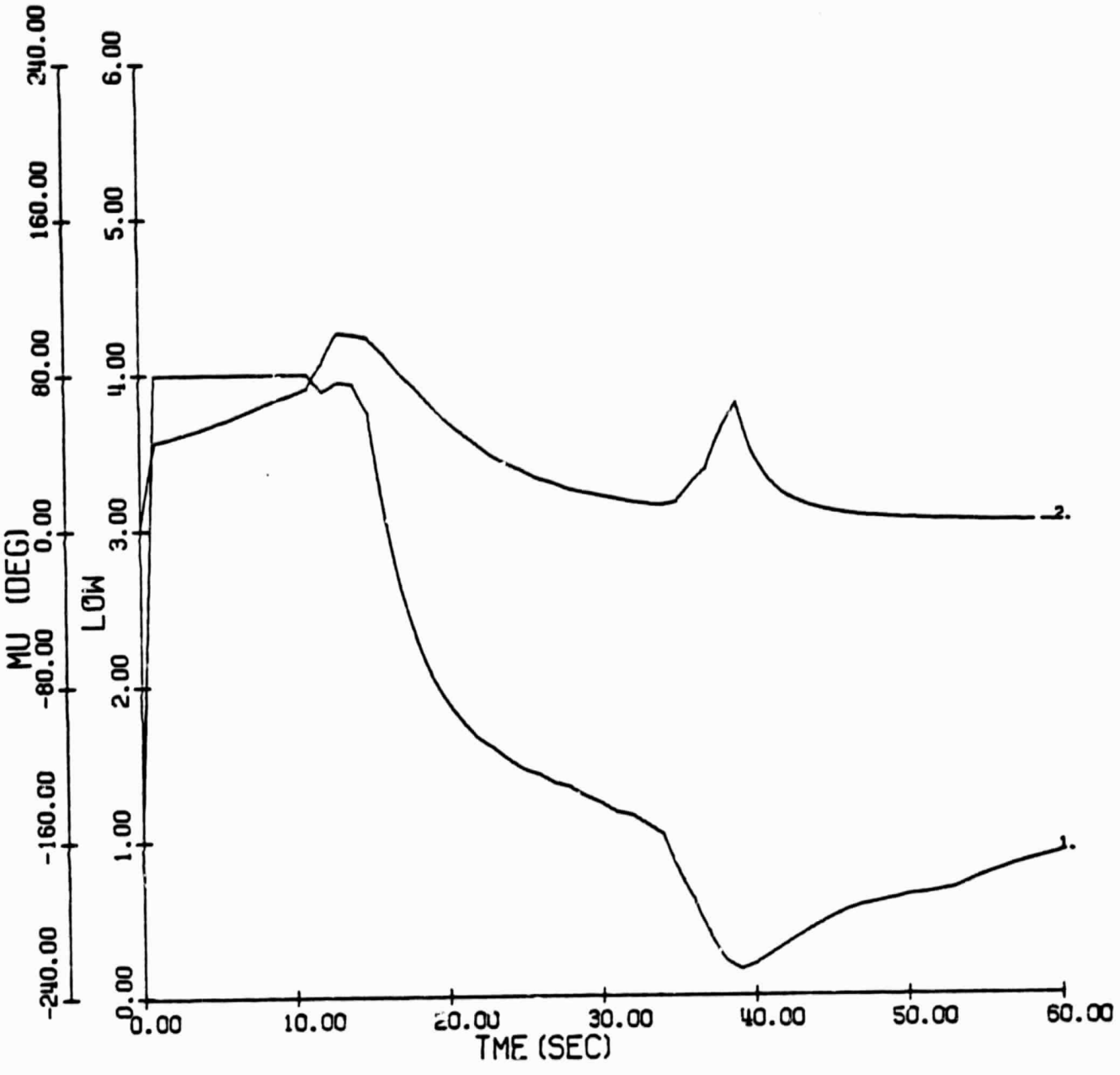

FIGURE 10. LIFT AND BANK ANGLE FOR CASE III WITH SUBOPTIMAL PROPORTIONAL CONTROL

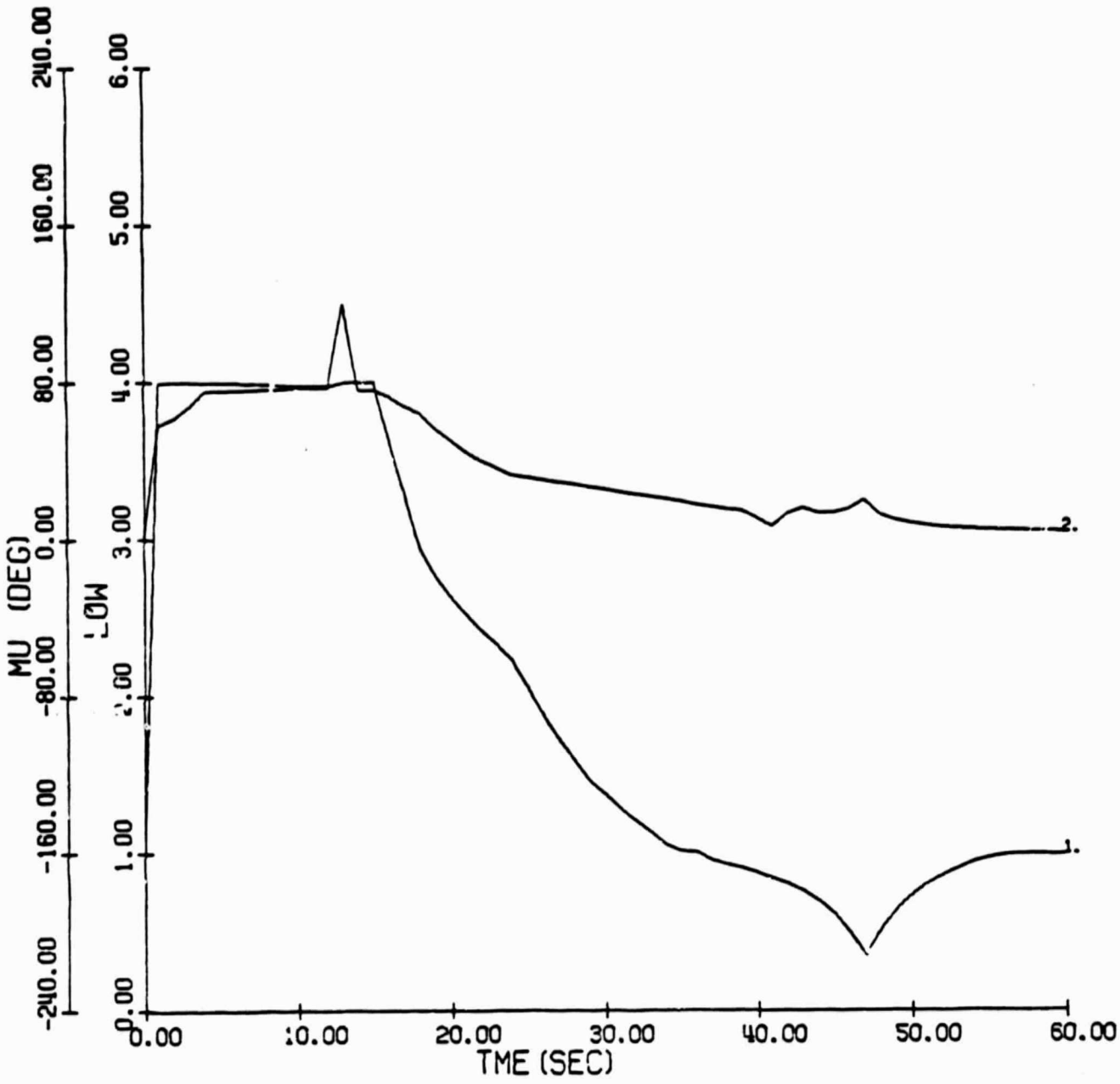

FIGURE 11. LIFT AND BANK ANGLE FOR CASE III WITH FULLY OPTIMIZED LIFT AND BANK ANGLE

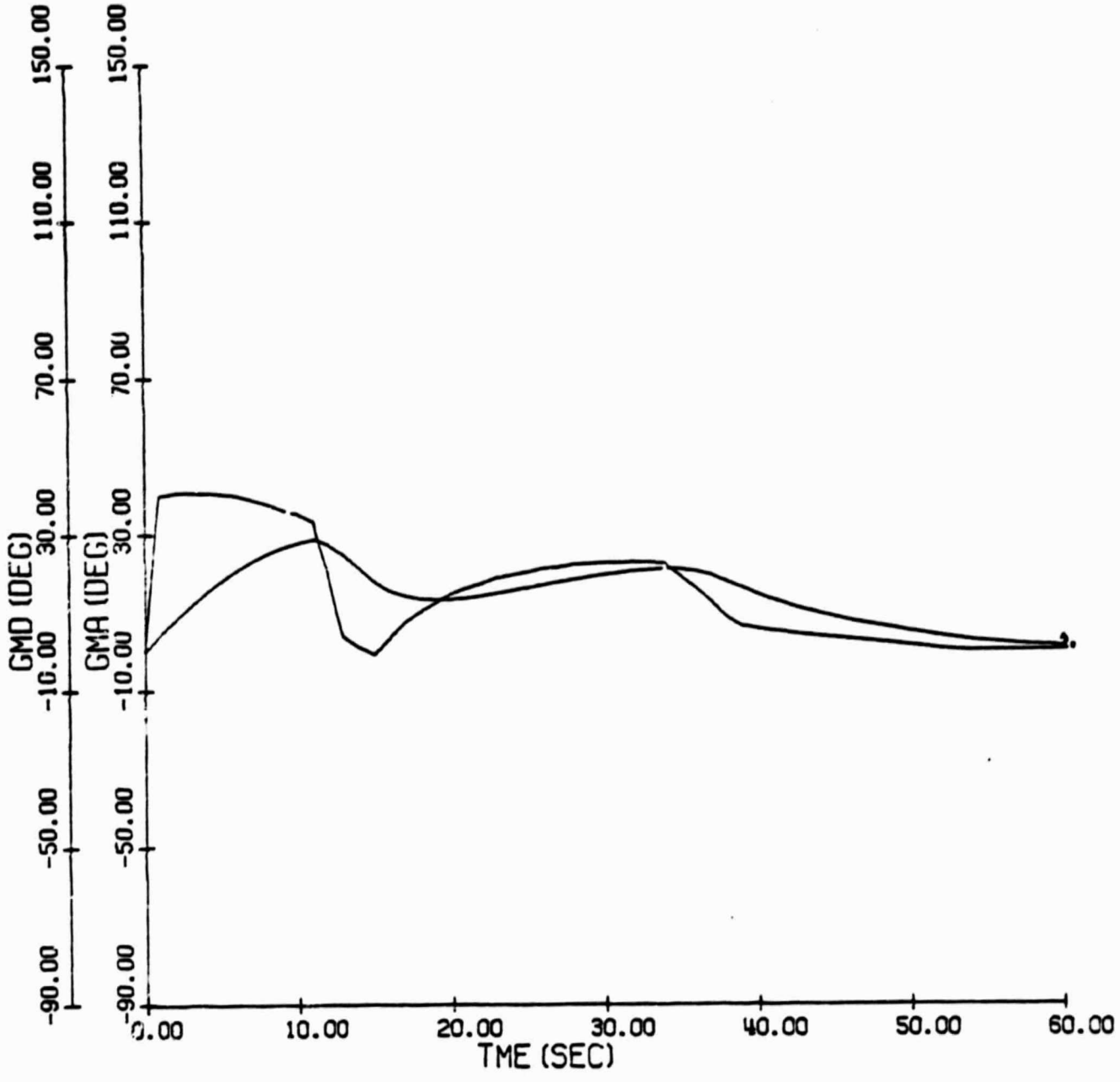

FIGURE 12. ACTUAL AND COMMANDED FLIGHT PATH ANGLE FOR CASE III WITH SUBOPTIMAL PROPORTIONAL CONTROL

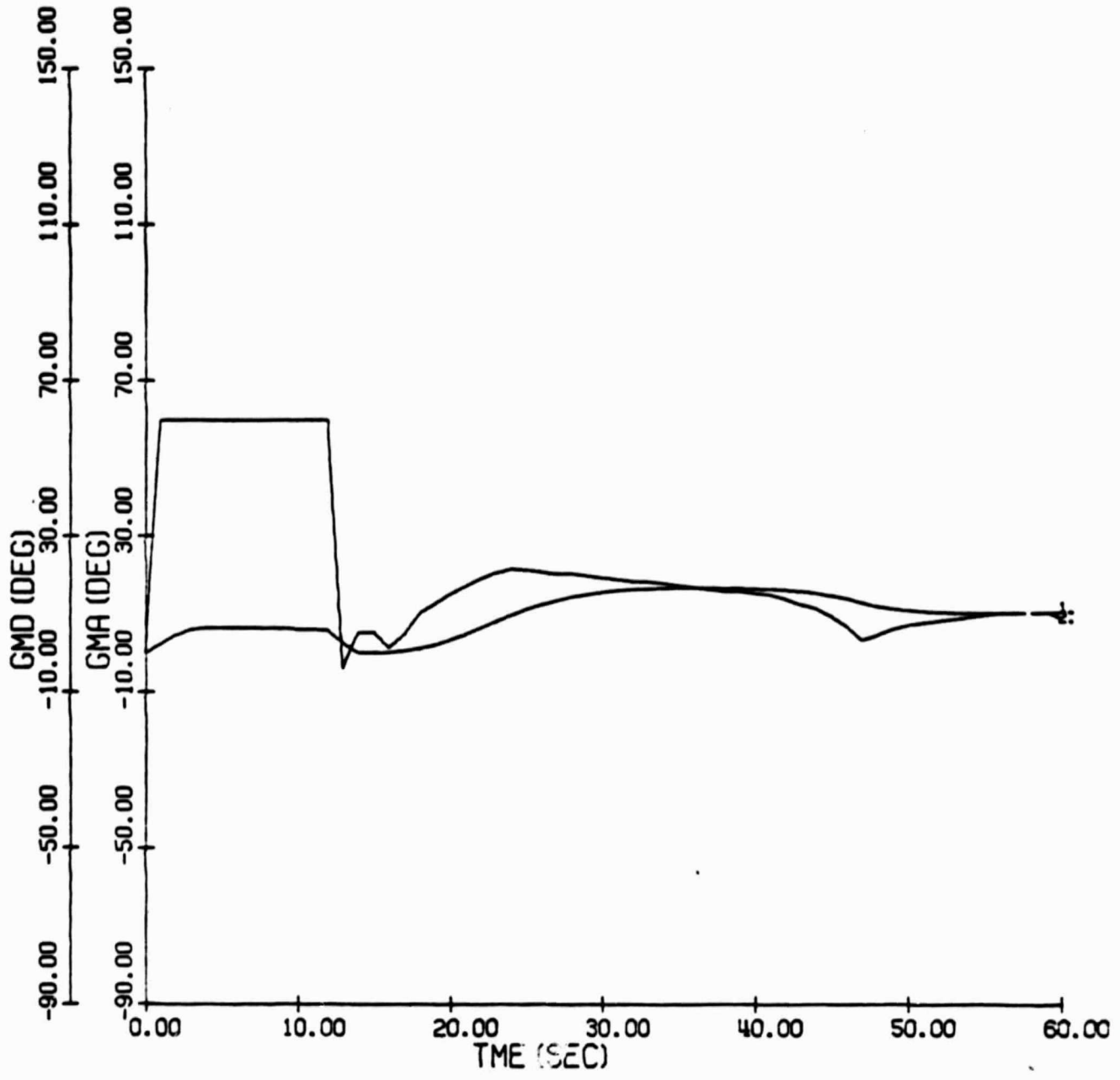

FIGURE 13. ACTUAL AND COMMANDED FLIGHT PATH ANGLE FOR CASE III WITH FULLY OPTIMIZED LIFT AND BANK ANGLE

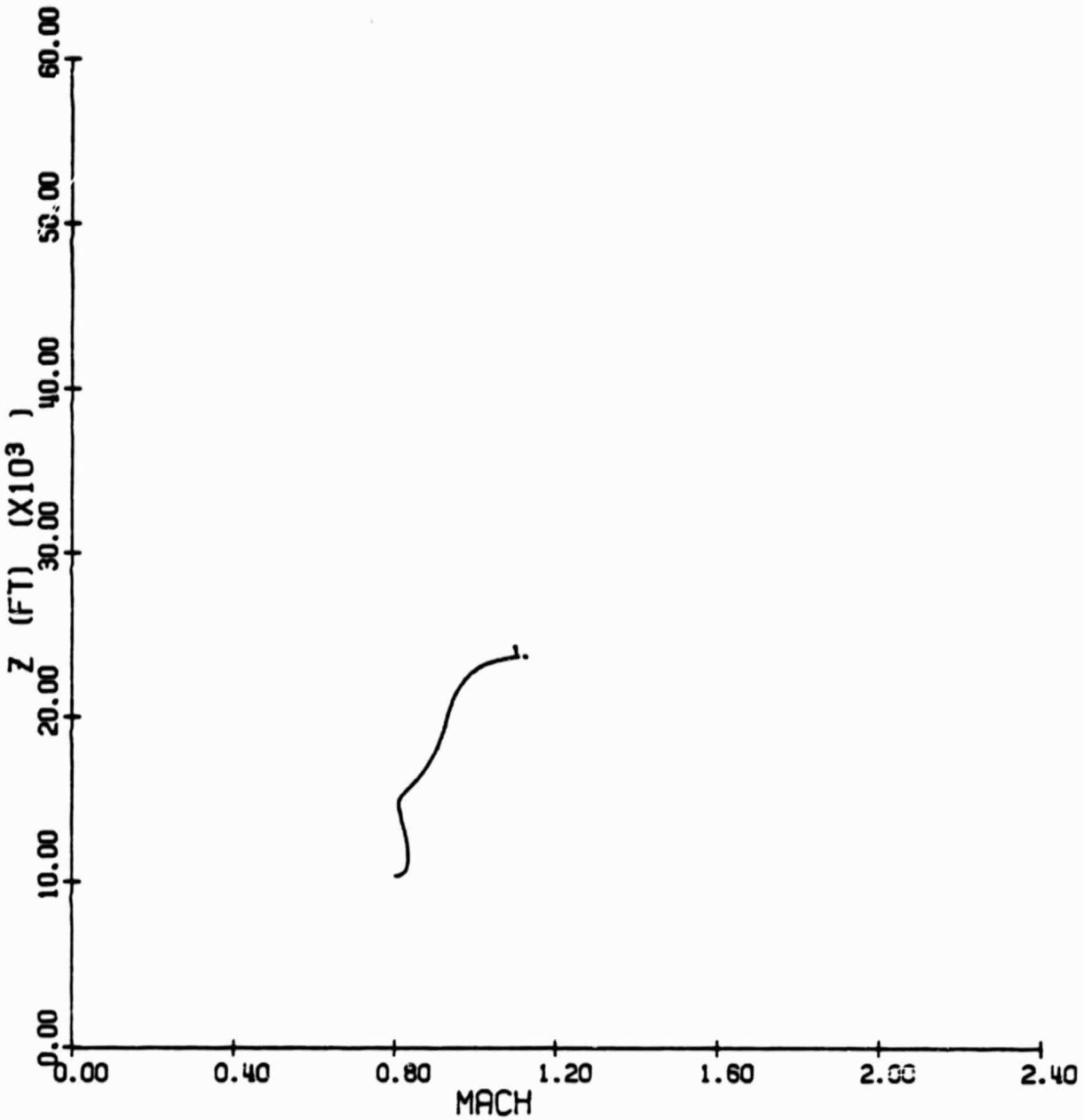

FIGURE 14. ALTITUDE VS MACH NUMBER FOR CASE III WITH SUBOPTIMAL PROPORTIONAL CONTROL

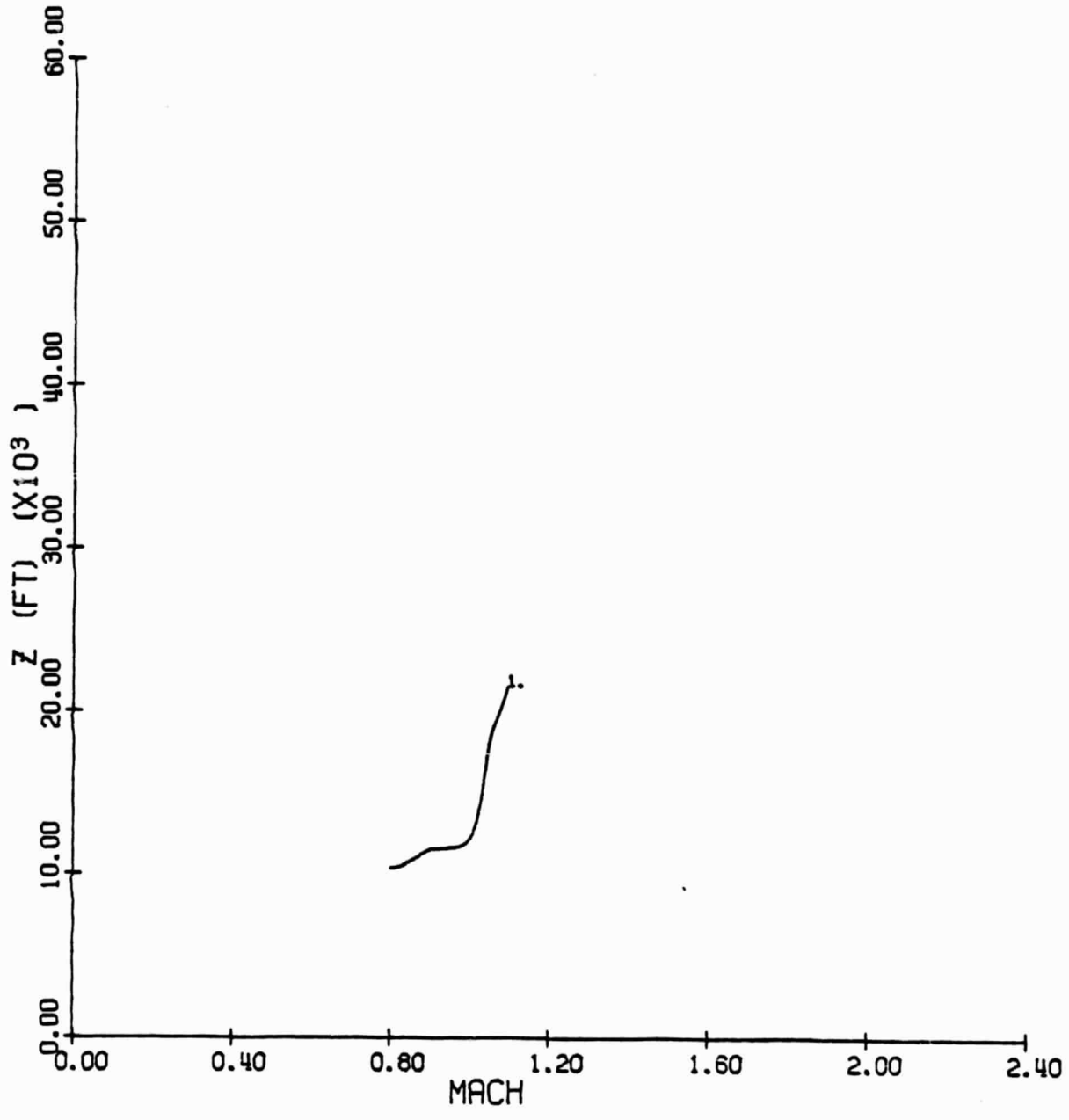

FIGURE 15. ALTITUDE VS MACH NUMBER FOR CASE III WITH FULLY OPTIMIZED LIFT AND BANK ANGLE

Cases for full control optimization is on the order of 2 seconds. An exact comparison will be made after modifications have been completed to avoid numerical difficulties, as cited above.

The development in [2] for range-matching to achieve optimal short range intercept was tested with initial geometries similar to Cases I and III from [2], placing the target at several values of initial range. The target altitude was set at 20,000 feet for these tests. Horizontal plane plots of the resulting trajectories are displayed in Figs. 16 to 21. The altitude histories and altitude versus mach plots for these tests are exhibited in Figs. 22 to 26.

An attempt was made to improve the aircraft's suboptimal tracking of optimal altitude commands through the implementation of a proportional-plus-integral scheme for vertical lift. This was motivated by the inability of the suboptimal proportional controller to accurately follow the first boundary layer descent path. For this aircraft, the optimal descent path lies along the maximum mach number boundary illustrated by the dashed line in Fig. 24. For the suboptimal control, this corresponds to a ramp in the commanded altitude requiring a type one controller for nulling the steady-state error. It is obvious from this figure that a proportional controller results in a steady-state altitude error during descent.

Initially, a simple addition of an integrator on altitude and error was added to the proportional scheme already in use in the manner described in Appendix B. This controller was tested on Case I-A. Profiles of actual and commanded altitude as functions of time are shown in Fig. 27 for the original proportional controller, while Fig. 28 reflects the inclusion of the integrator. The considerable instability exhibited in Fig. 28 was due to coupling between flight path angle (γ) and energy rate ($\dot{E}$) dynamics described more fully in Appendix B. On the basis of this problem, the controller was reformulated with time

constants compensated as functions of energy in the manner described in Appendix B. This formulation was tested in the same manner as the first, resulting in the altitude profile displayed in Fig. 29. With the encouragement of enhanced stability and greatly reduced errors, the controller was tested on Case I-A to intercept. Unfortunately, the controller became completely unstable at cruise due to large coupling between energy rate dynamics and lift in that region, this being due to an extremely low energy rate. Weighing the difficulties anticipated in solving this problem against the expected benefits, no further work will be done in this area.

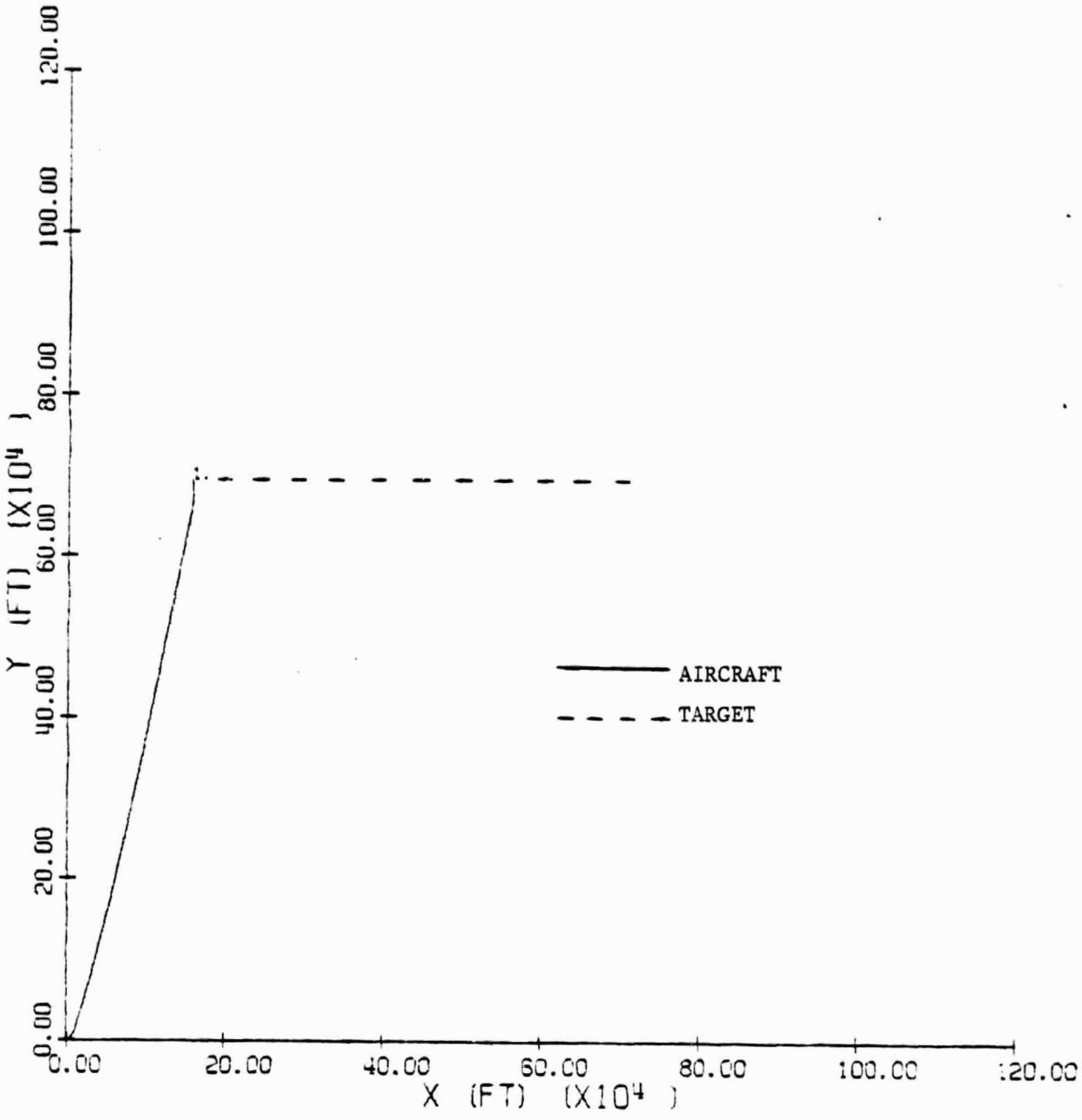

FIGURE 16. HORIZONTAL PLANE TRAJECTORY OF CASE I LONG RANGE INITIAL RANGE TO TARGET (R_o) = 1.2 X 10^6 FT.

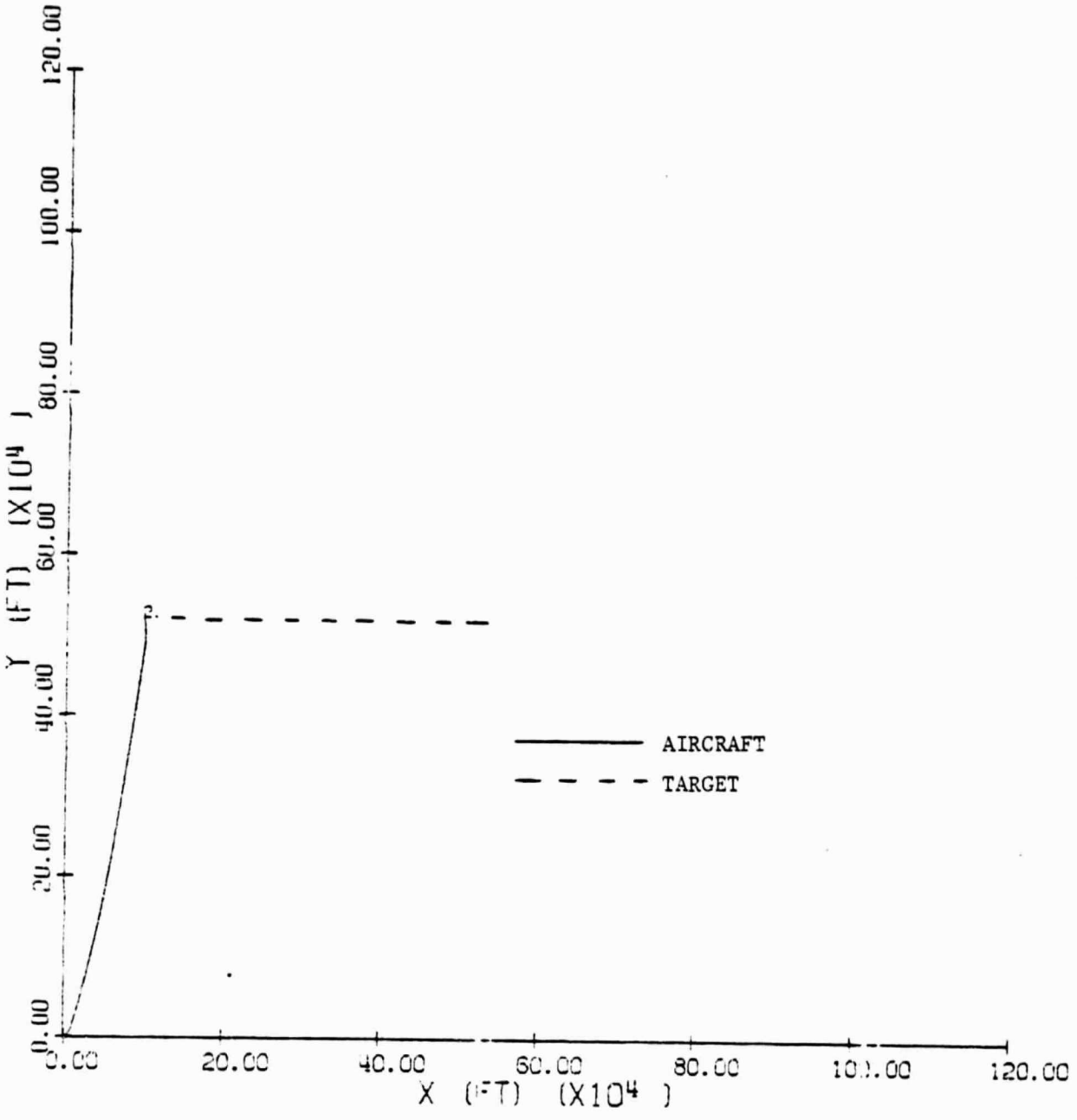

FIGURE 17. HORIZONTAL PLANE TRAJECTORY OF CASE I SHORT RANGE

INITIAL RANGE TO TARGET = 0.75 R_o

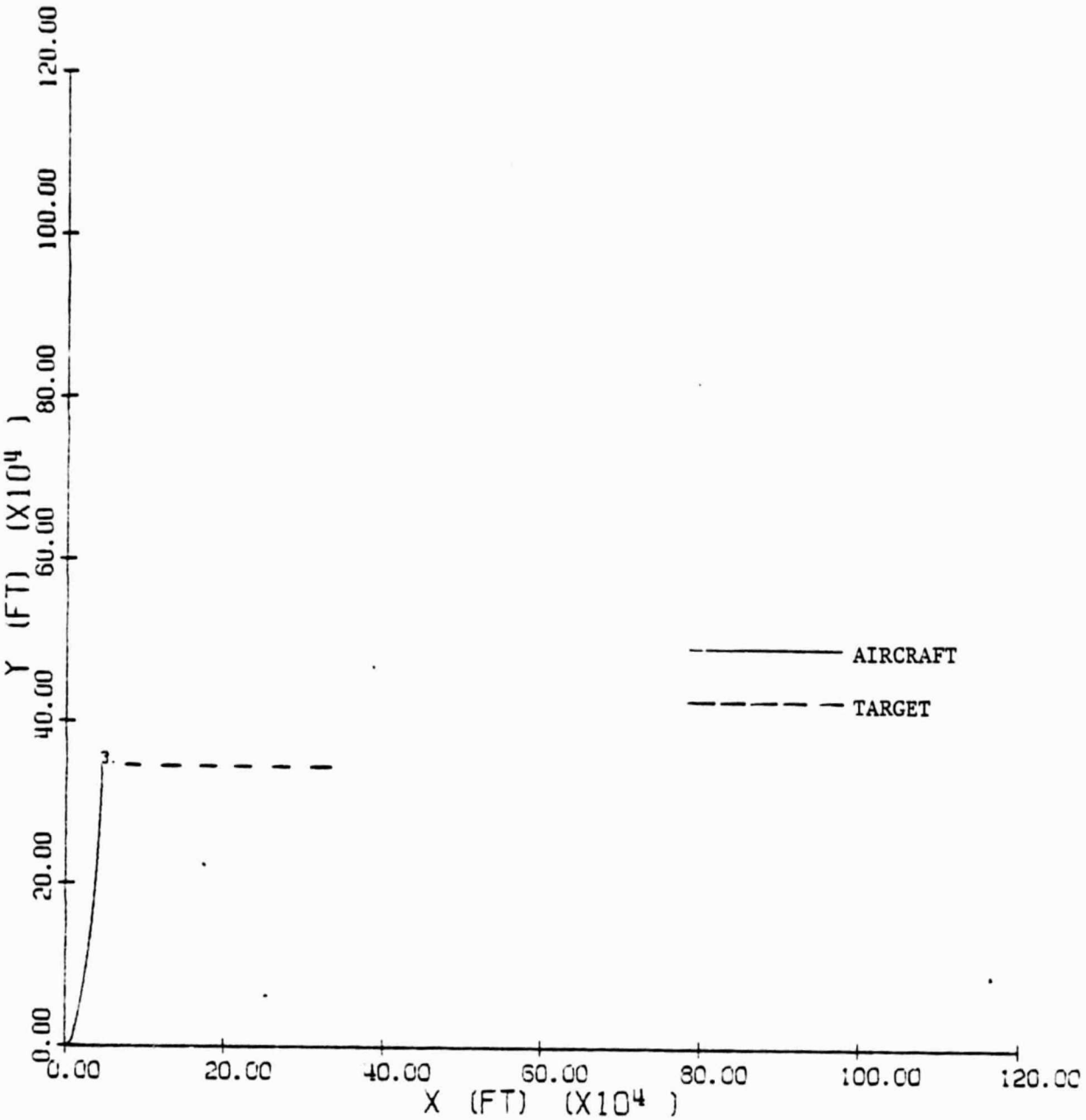

FIGURE 18. HORIZONTAL PLANE TRAJECTORY OF CASE I SHORT RANGE

INITIAL RANGE TO TARGET = 0.5 R_o

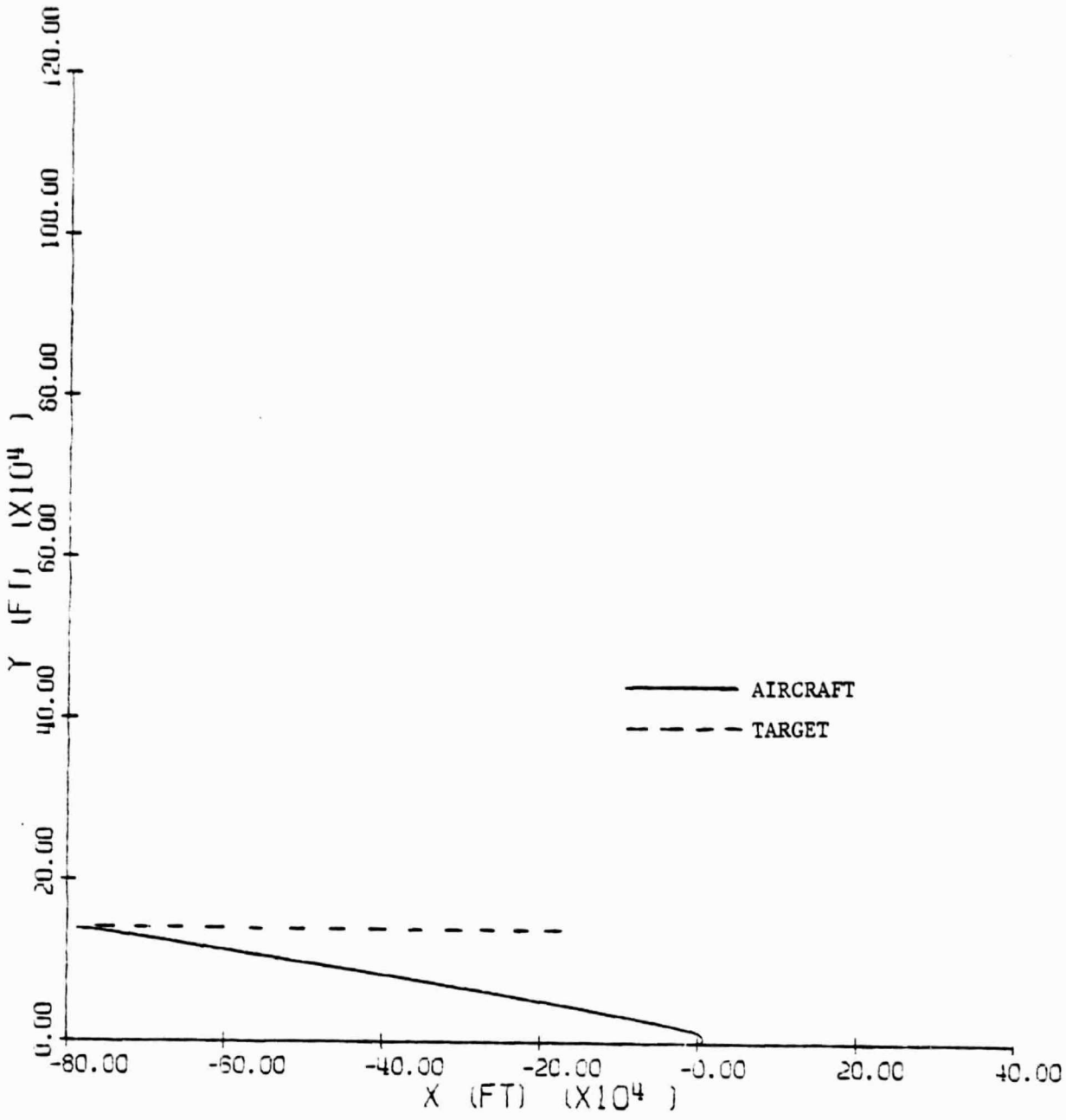

FIGURE 19. HORIZONTAL PLANE TRAJECTORY OF CASE III LONG RANGE INITIAL TARGET X-COORDINATE = -1800 FT.

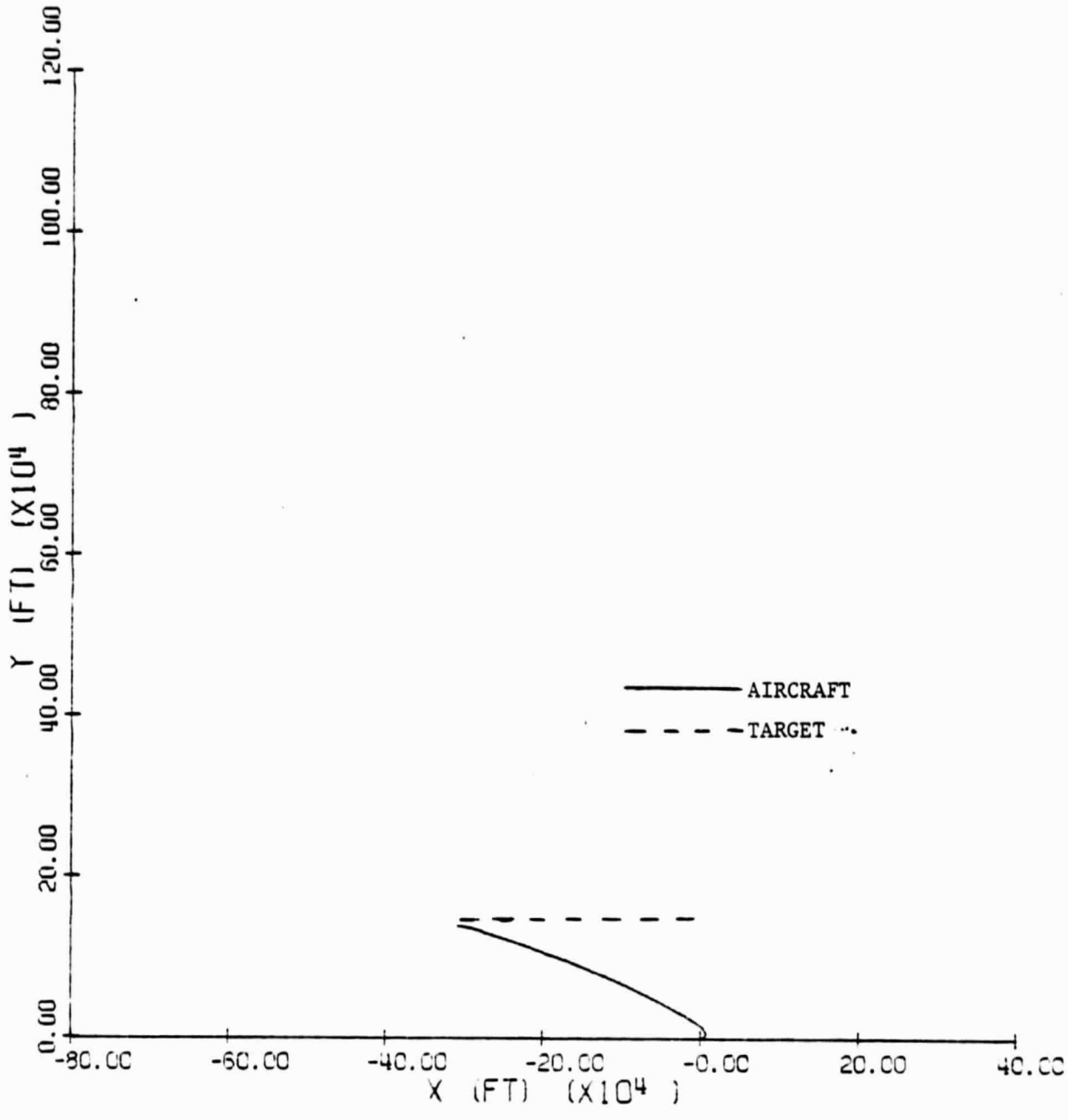

FIGURE 20. HORIZONTAL PLANE TRAJECTORY OF CASE III SHORT RANGE

INITIAL TARGET X-COORDINATE = 0 FT.

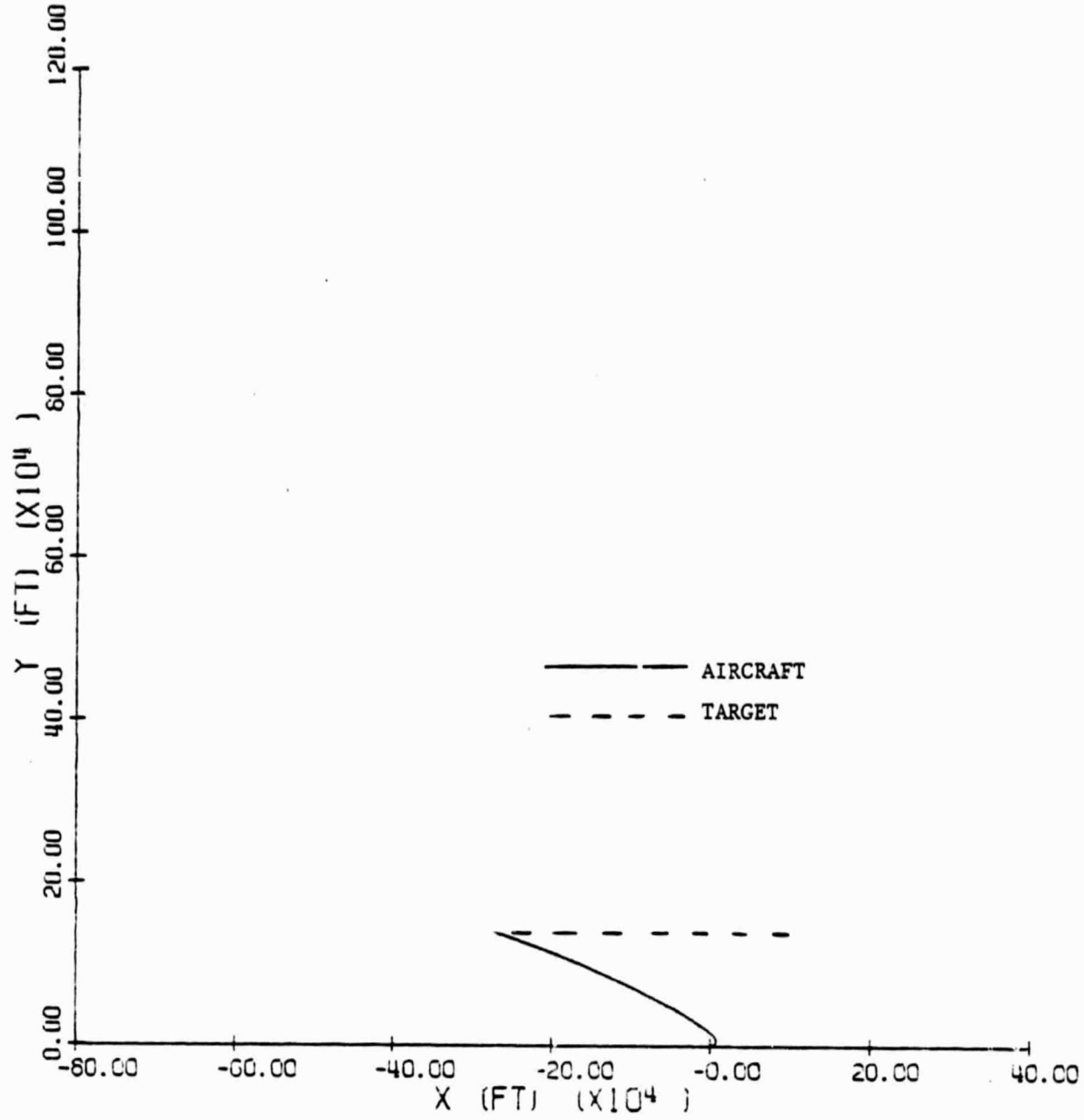

FIGURE 21. HORIZONTAL PLANE TRAJECTORY OF CASE III SHORT RANGE

INITIAL TARGET X-COORDINATE = 1000 FT.

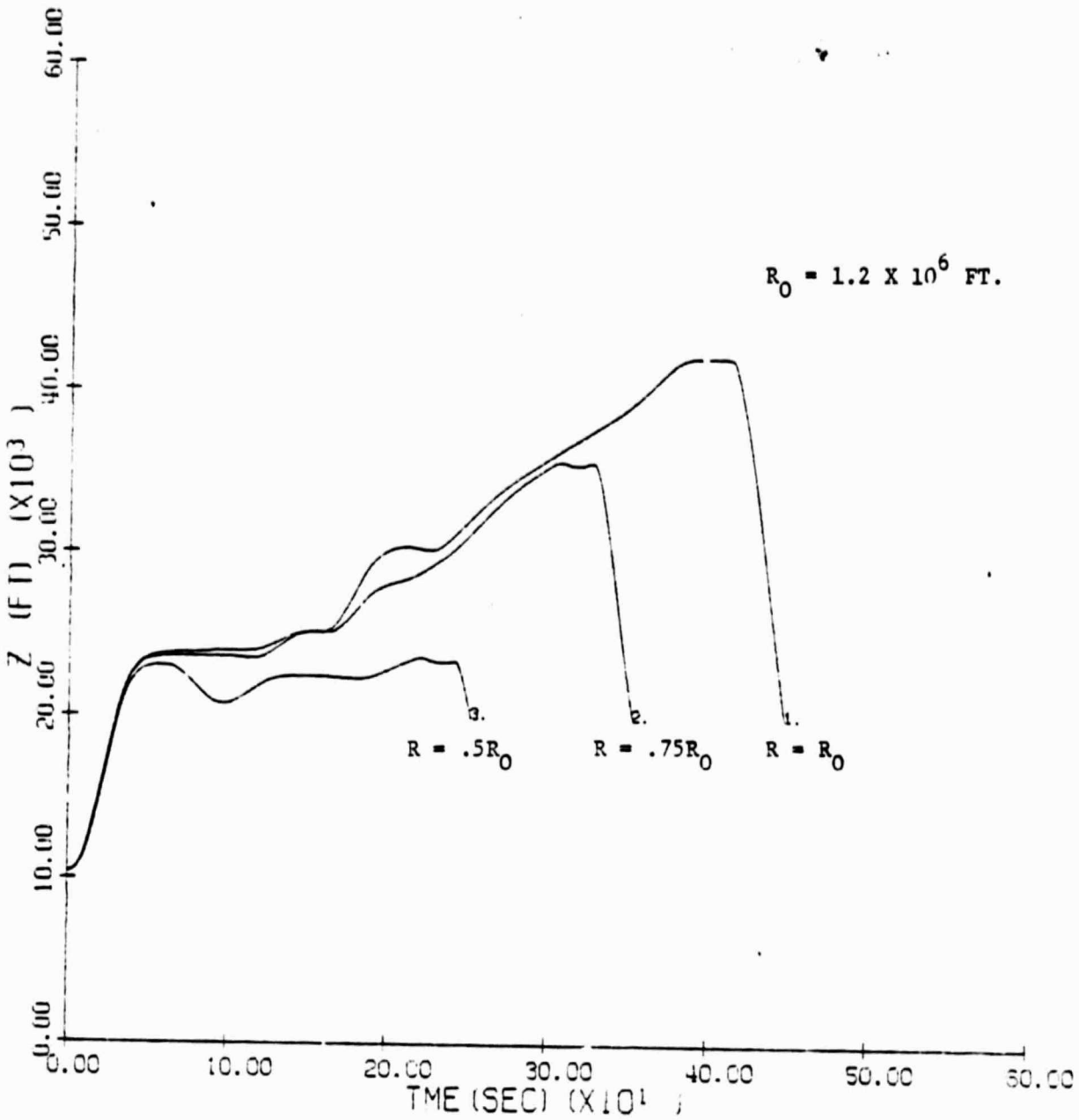

FIGURE 22. ALTITUDE PROFILES FOR CASE I FOR SEVERAL VALUES OF INITIAL RANGE

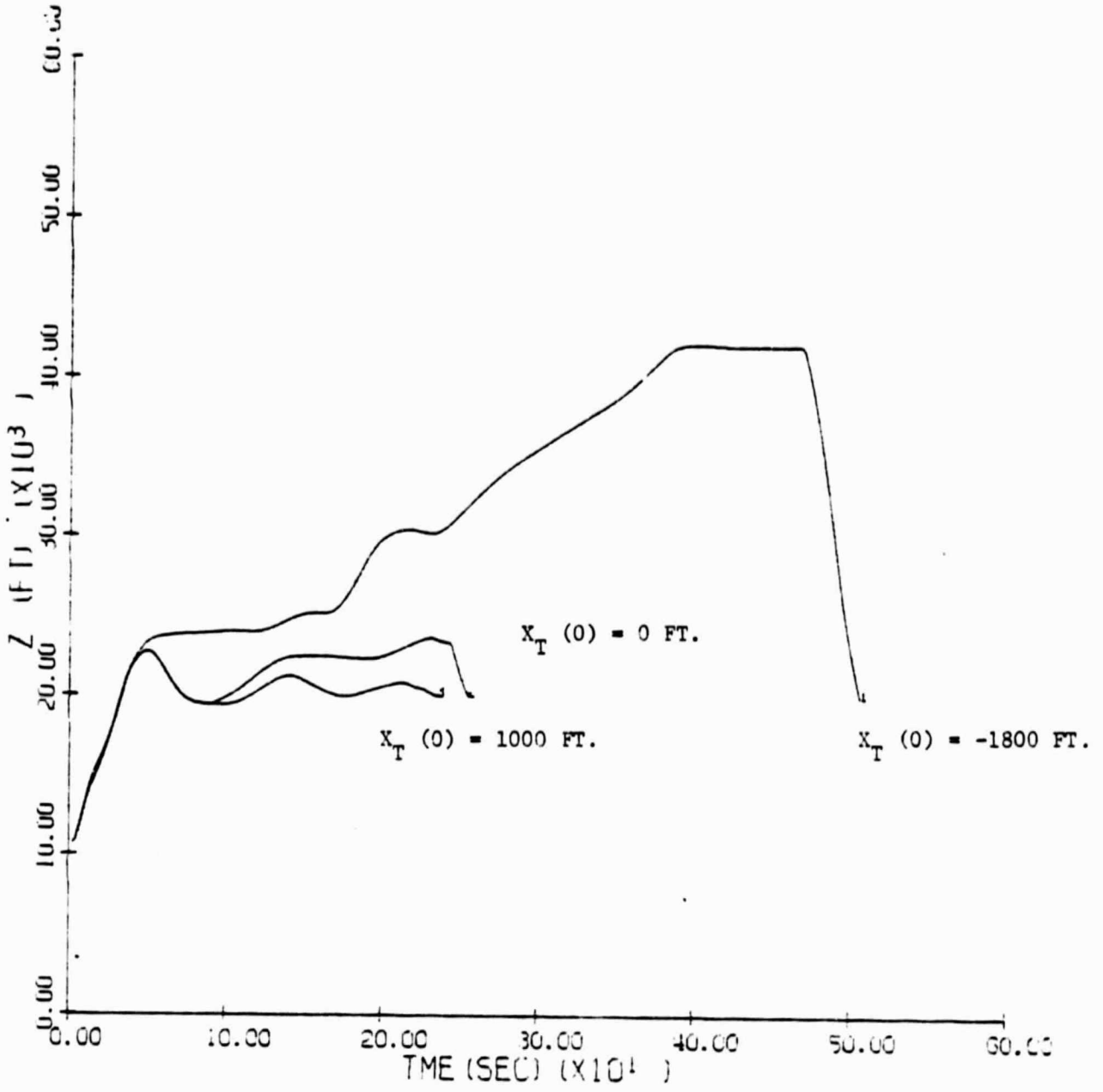

FIGURE 23. ALTITUDE PROFILES FOR CASE III FOR SEVERAL VALUES OF INITIAL TARGET DOWN RANGE POSITION

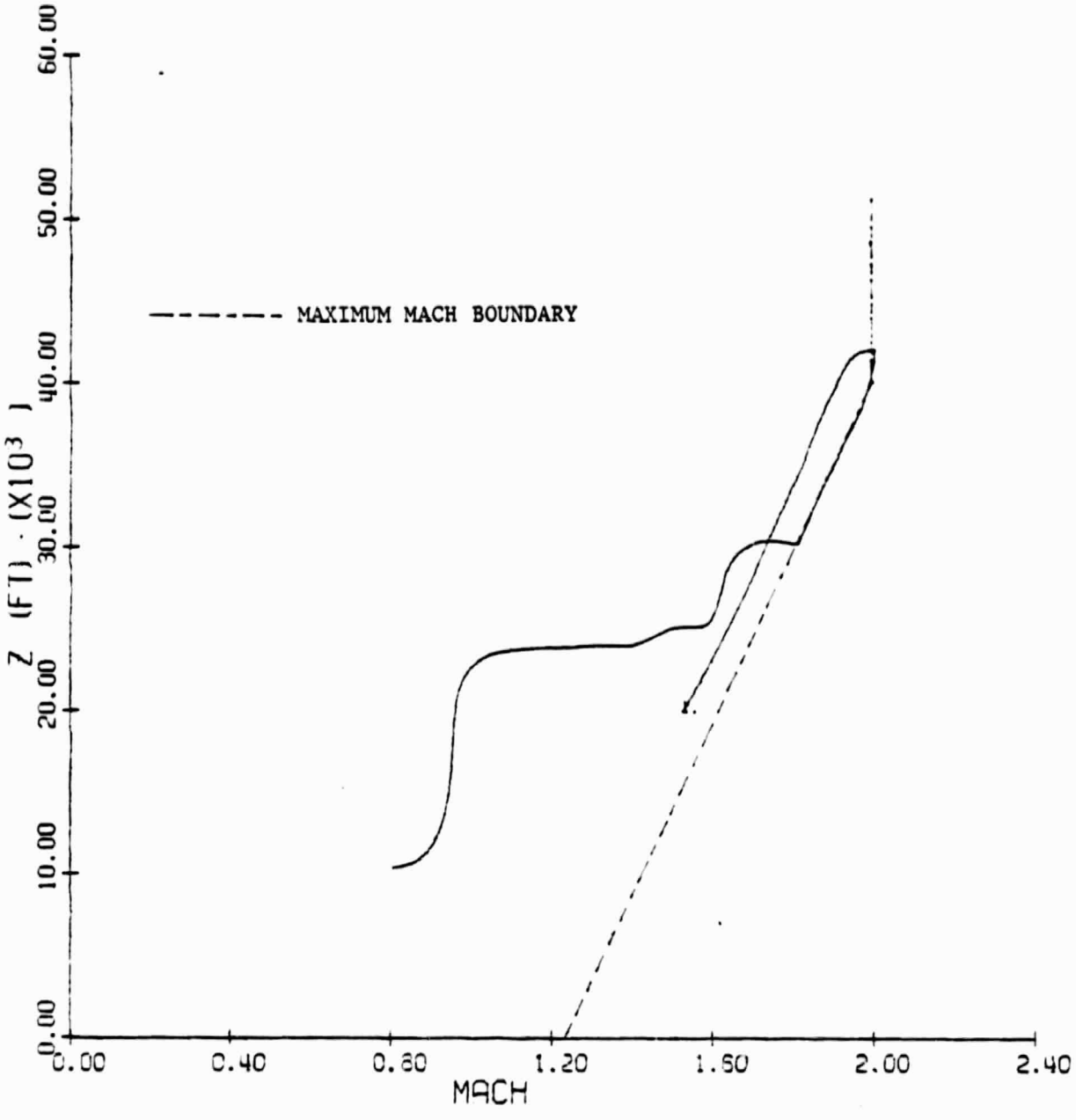

FIGURE 24. ALTITUDE VS MACH NUMBER FOR CASE I LONG RANGE

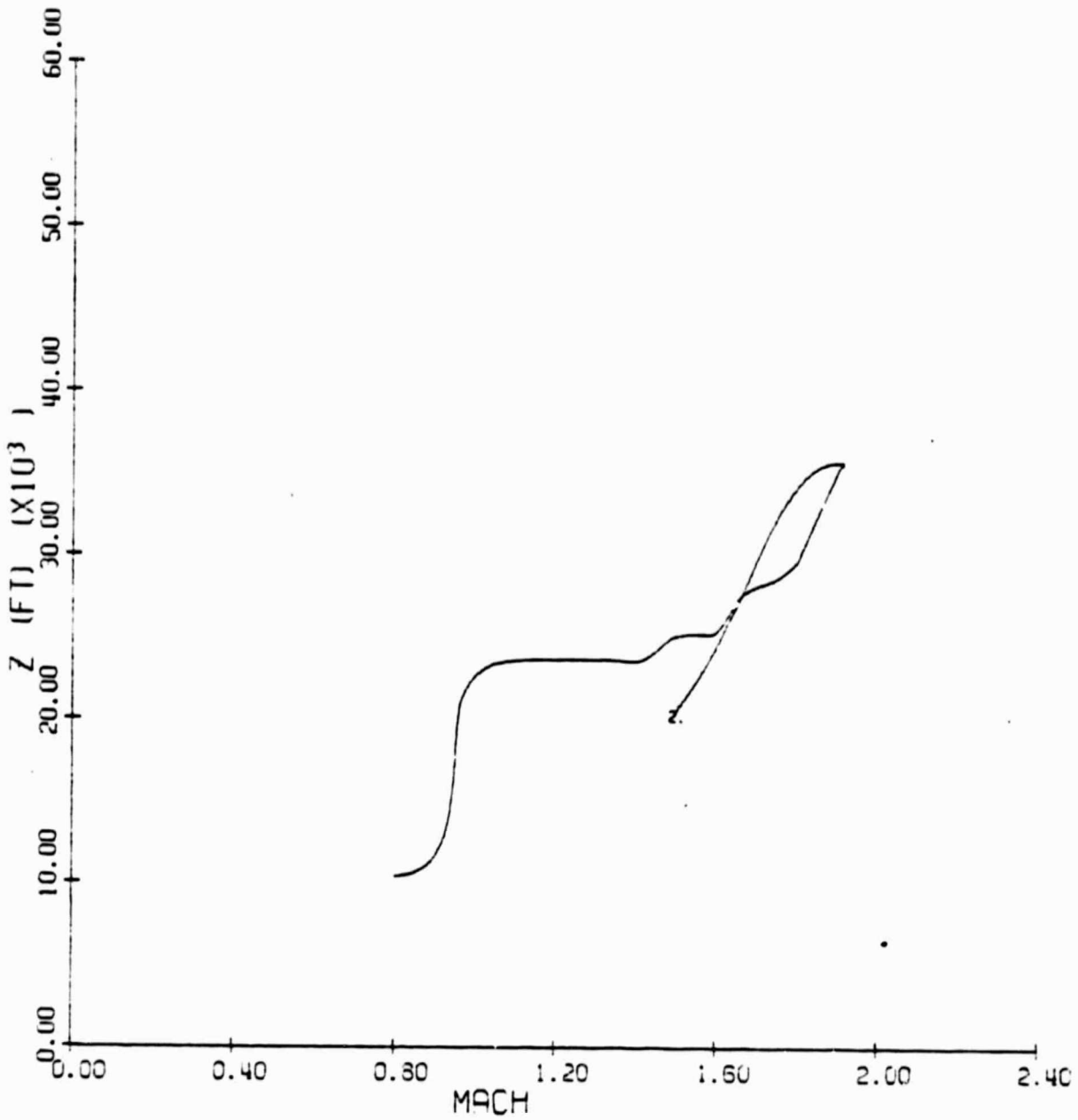

FIGURE 25. ALTITUDE VS MACH NUMBER FOR CASE I SHORT RANGE

INITIAL RANGE TO TARGET = 0.75 R_o

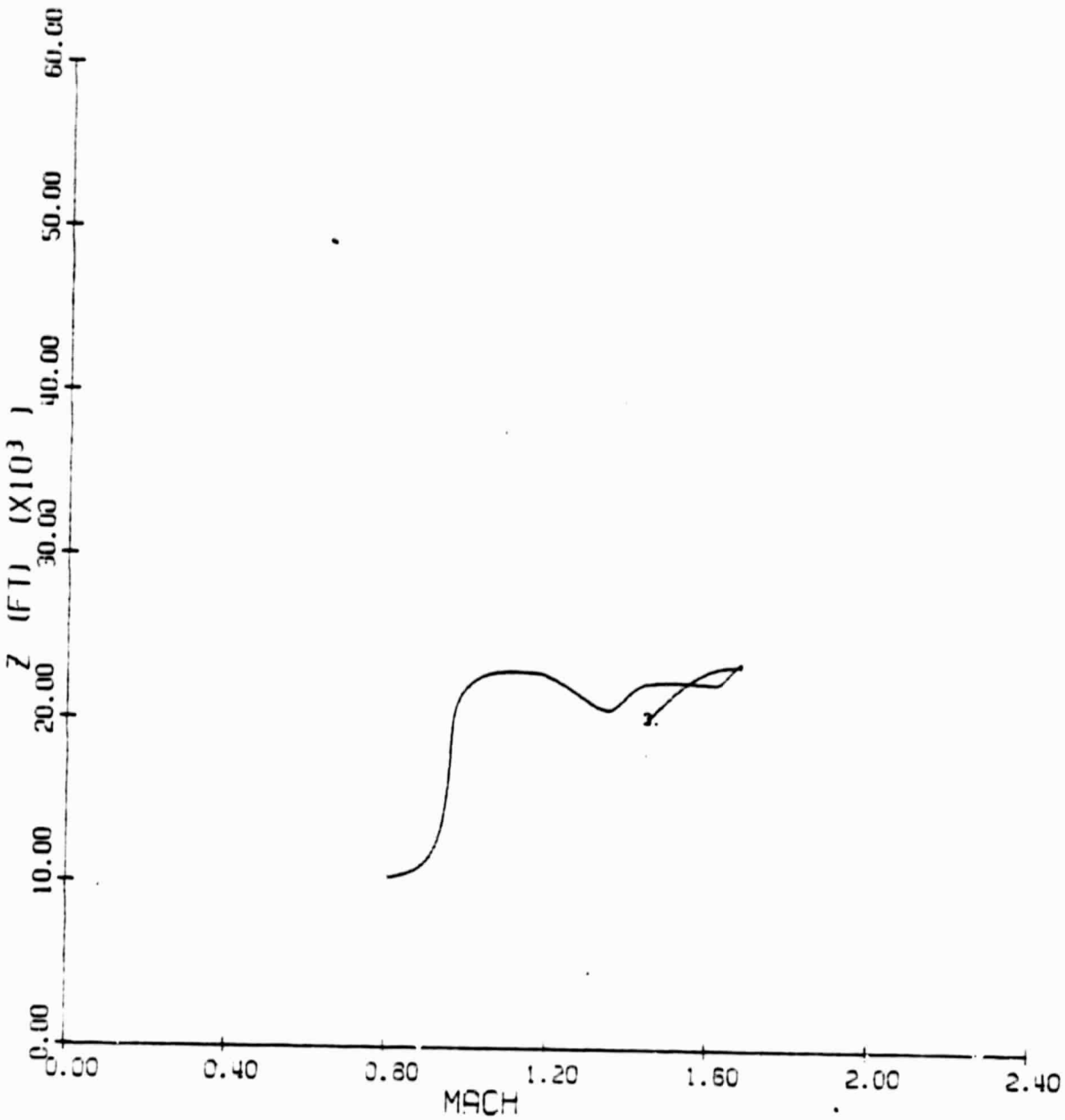

FIGURE 26. ALTITUDE VS MACH NUMBER FOR CASE I SHORT RANGE

INITIAL RANGE TO TARGET = 0.5 R_o^*

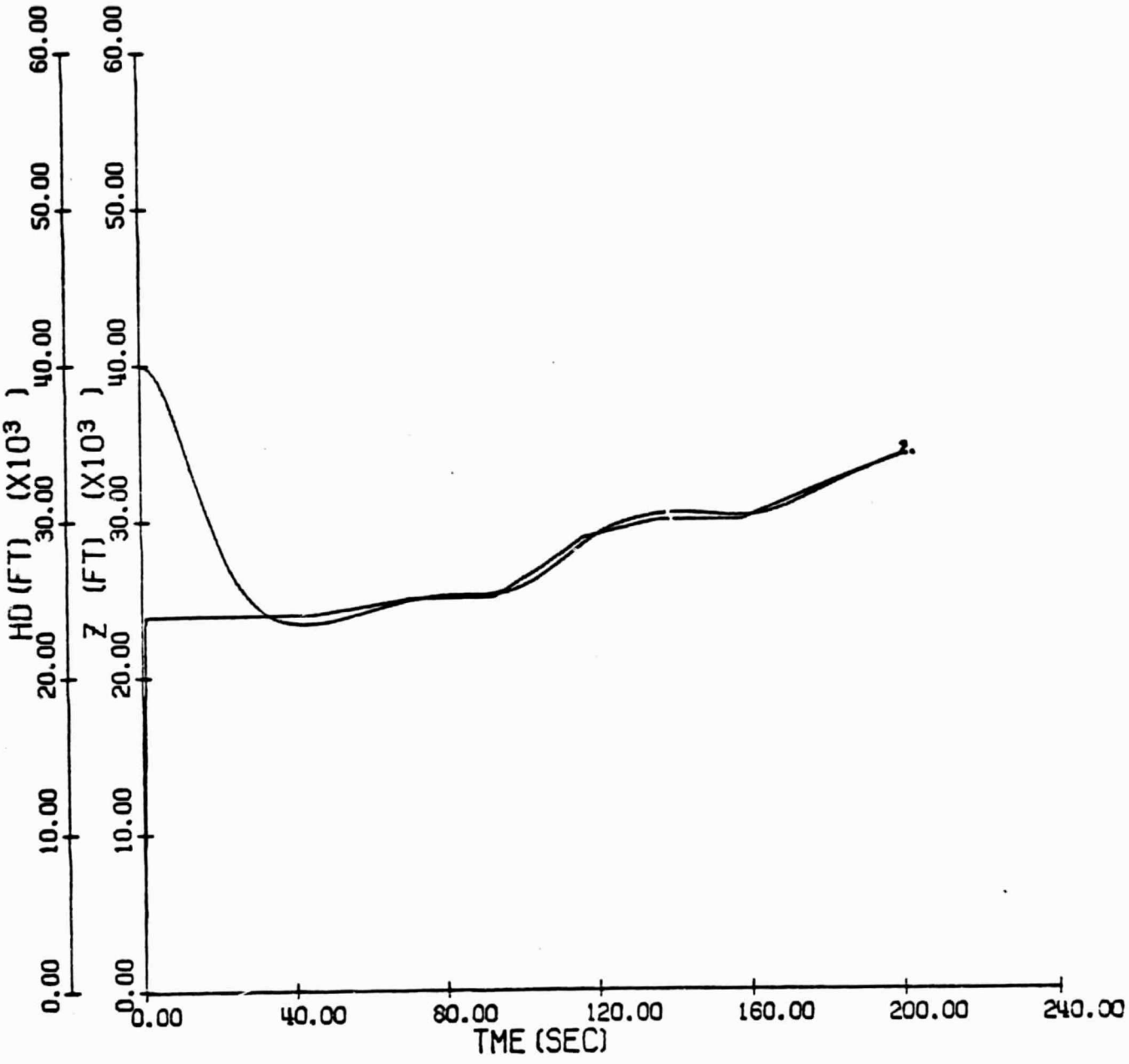

FIGURE 27. ACTUAL AND COMMANDED ALTITUDE FOR CASE I-A WITH PROPORTIONAL SUBOPTIMAL CONTROL.

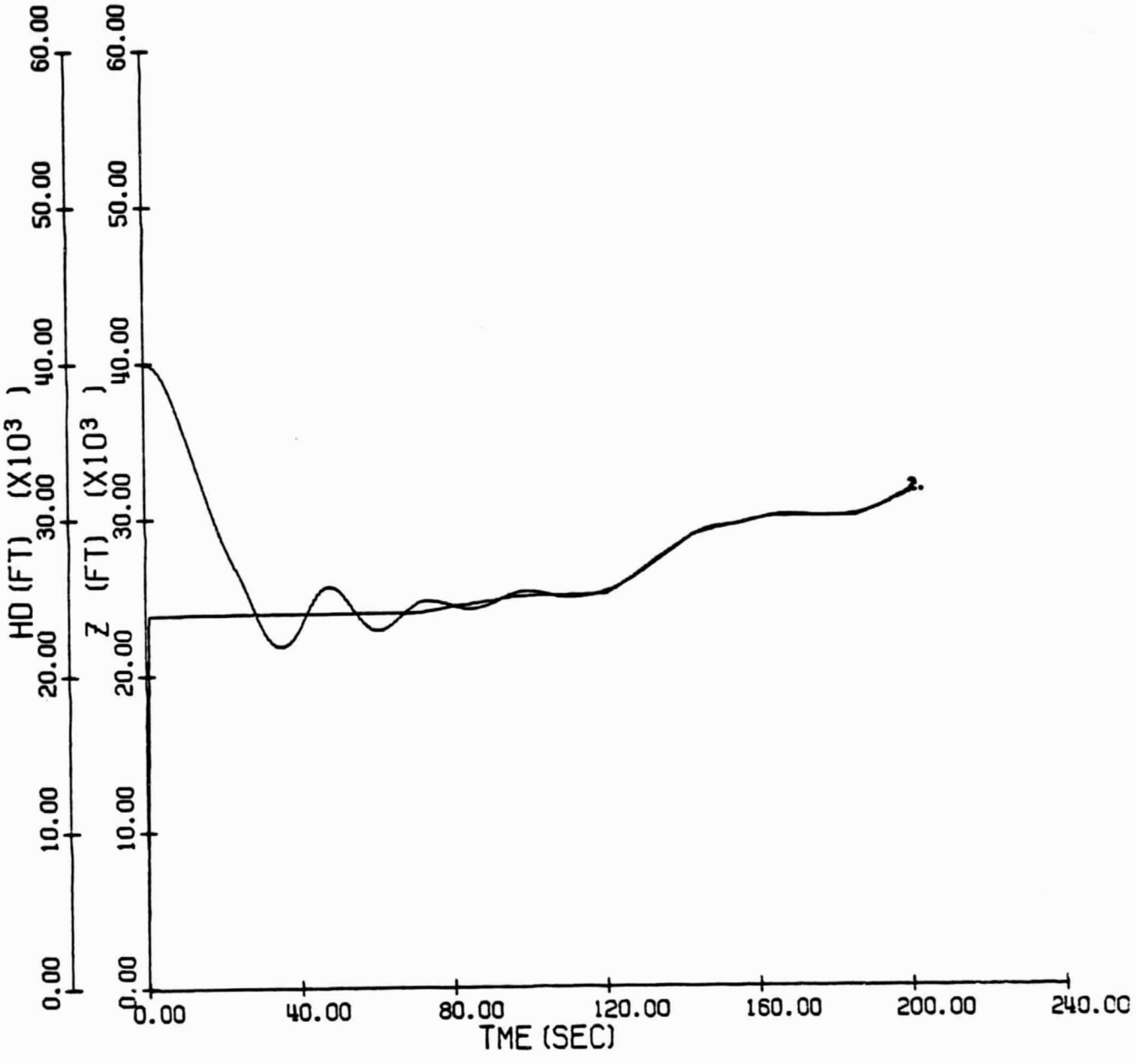

FIGURE 28. ACTUAL AND COMMANDED ALTITUDE FOR CASE I-A WITH UNCOMPENSATED P-I SUBOPTIMAL CONTROL

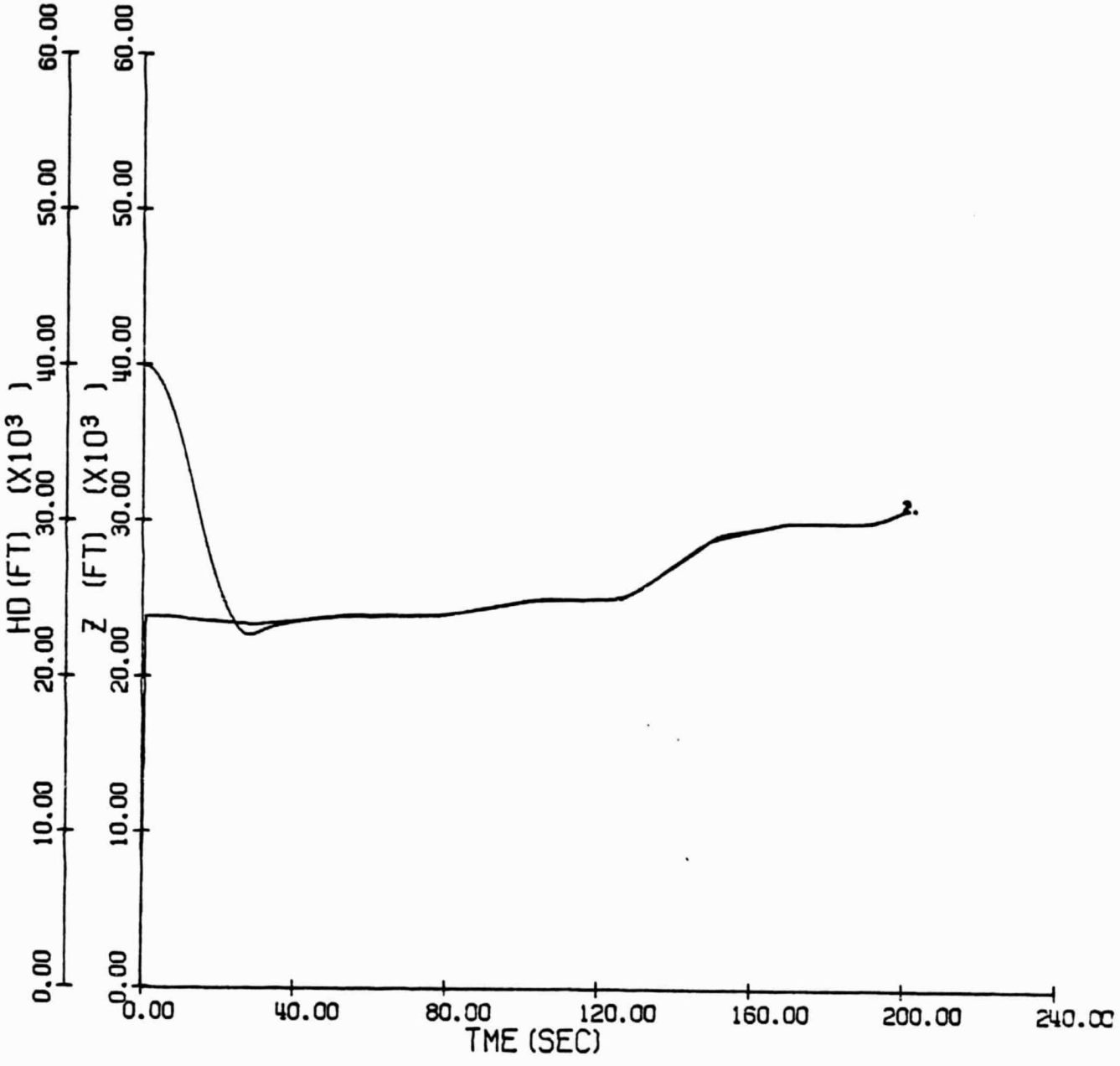

FIGURE 29. ACTUAL AND COMMANDED ALTITUDE FOR CASE I-A WITH COMPENSATED P-I SUBOPTIMAL CONTROL

APPENDIX A

This appendix proves that the roots of the quadratic expression for λ_γ obtained in (23) of section 3.1 are always real and of opposite sign. It will also be shown that the fourth boundary layer controls are asymptotic to those of the third.

From section 3.1 we have that, on the lift constraint

$$A\lambda_\gamma^2 + B\lambda_\gamma^2 + C = 0 \tag{A-1}$$

where

$$A = g^2[L_{max}{}^2/W^2 - \cos^2 \gamma]/V^2 \tag{A-2}$$

$$B = 2\Phi g \cos \gamma/V \tag{A-3}$$

$$C = [\lambda_{\beta_2} L_{max} g/VW \cos \gamma]^2 - \Phi^2 \tag{A-4}$$

$$\Phi = H_1(h,E,\beta,\gamma,L = L_{max}) + \lambda_{h_3} V \sin \gamma \tag{A-5}$$

where H_1 has been defined in (5).

The roots of (A-1) are as follows:

$$\lambda_{\gamma_{1,2}} = [-B \pm \sqrt{B^2 - 4AC}\,]/2A \tag{A-6}$$

where the term under the radical is

$$B^2 - 4AC = 4[(\Phi L_{max} g/VW)^2 - (\Phi L_{max} g/VW) - (\lambda_{\beta_2} L_{max} g^2/WV^2)^2 + (\lambda_{\beta_2} (L_{max} g/VW)^2/\cos \gamma)^2] \tag{A-7}$$

For the value of this expression to remain non-negative it is necessary that

$$\phi^2 + [1 - (L_{max}/W \cos \gamma)^2] [\lambda_{\beta_2} g/V]^2 \geq 0 \qquad \text{(A-8)}$$

or

$$\phi^2 \geq [L_{max}^2 - W^2 \cos^2 \gamma] [\lambda_{\beta_2} g/VW \cos \gamma]^2 \qquad \text{(A-9)}$$

In the third boundary layer it can be seen that

$$L_{n_{max}}^2 = L_{max}^2 - W^2 \cos^2 \gamma \qquad \text{(A-10)}$$

Also, the third boundary layer Hamiltonian in (4), evaluated at the conditions under consideration is

$$H_3 = \phi + \lambda_{\beta_2} L_{n_{max}} g/VW \cos \gamma \geq 0 \qquad \text{(A-11)}$$

The product $\lambda_{\beta_2} \cdot L_n$ is always negative, so (A-10) can be rewritten

$$\phi \geq | \lambda_{\beta_2} L_{n_{max}} g/VW \cos \gamma | \qquad \text{(A-12)}$$

Combining (A-10) and (A-12) gives us (A-9) assuring us that the roots of (A-1) are real.

Adressing the signs of the roots (A-6), it is obvious that, in the quadratic formula, the term under the radical must have a dominating magnitude for two different signs to occur. This is tantamount to requiring that

$$AC \leq 0 \qquad \text{(A-13)}$$

Since it can be seen from (A-2) that $A \geq 0$ where $L_{max} \geq W$, then we must have that

$$C \leq 0 \qquad \text{(A-14)}$$

From (A-4) and (A-12) it can be seen that this is indeed the case.

Finally, to prove the asymptotic behavior of the fourth boundary layer

controls, we will show that δL_1 and δL_n both tend to zero as the current flight path angle approaches its third boundary layer optimal value (γ_3). From the fourth boundary layer analysis we have that, off the lift constraint

$$\delta L_{n_4} = [\lambda_{\beta_2} qsg/2\lambda_{E_1} KV^2 \cos \gamma - L_{n_3}] \tag{A-15}$$

$$\delta L_{14} = [-H_3 qsW/\lambda_{G_1} KV - \delta^2 L_{n_4}]^{1/2} \tag{A-16}$$

We note from (8) that values of L_{n_3} satisfying $\partial H/\partial L_n = 0$ off the lift constraint are

$$L_{n_3} = \lambda_{\beta_2} qsg/2\lambda_{E_1} KV^2 \cos \gamma_3 \tag{A-17}$$

It is evident from the above that δL_{n_4} in (A-15), being continuous, will asympotically approach zero as the current flight path angle (γ) $\rightarrow \gamma_3$. Turning to δL_{14} in (A-16) it seen that δL_{n_4} and H_3 will both approach zero $\gamma \rightarrow \gamma_3$

APPENDIX B

This appendix documents the derivation of a proportional-plus-integral scheme for sub-optimally computing vertical lift in the simulation. Figure B-1 illustrates a straightforward addition of a term integrating $(h_c - h)$ to the proportional controller shown in Figure 6 of [2]. This approach proved unsatisfactory due to the interaction of vertical lift with aircraft energy rate, which was not accounted for, and which resulted in unstable behavior. The dashed line in Figure 1 models the effect of vertical lift (L_1) on energy rate ($\dot{E}$), and is seen to act as an outer loop around the original model for the third order P-I controller.

On the basis of this the control gains K_I, K_γ and K_h, defined by[+]

$$K_I = 1/\tau_I \tag{B-1}$$

$$K_\gamma = 1/\tau_\gamma \tag{B-2}$$

$$K_h = 1/\tau_h \tag{B-3}$$

were redisigned to account for $\dot{E}$ dynamics. The term $h_c(E)$ represents the optimum climb (descent) altitude schedule as a function of energy level.

A linearized perturbation block diagram is shown in Figure B-2. The linearization is about L = W, where

$$K_E = \partial h_c/\partial E \tag{B-4}$$

$$K_{\dot{E}} = -\partial\dot{E}/\partial E = 2KV/qs \tag{B-5}$$

The characteristic equation for this system is given by

[+] τ_h and τ_γ here correspond to τ_1 and τ_2 in Figure 6 of [2].

$$s^3 + [K_\gamma + aK_\gamma K_h]s^2 + K_\gamma[K_h + aK_I]s + K_\gamma K_I = 0 \qquad \text{(B-6)}$$

where

$$a = mK_E K_{\dot{E}} \cos \gamma \qquad \text{(B-7)}$$

If we arrange the poles of the system according to

$$(s + K_1)\ (s^2 + K_2 s + K_3) = 0 \qquad \text{(B-8)}$$

where

$$K_1 \geq 10\ \omega_n \qquad \text{(B-9)}$$

$$K_2 = 2\xi\omega_n \qquad \text{(B-10)}$$

$$K_3 = \omega_n^2 \qquad \text{(B-11)}$$

then we can compute the gains equating the coefficients of like powers of s in (B-6) and (B-8):

$$K_\gamma = K_1 + K_2 - a(K_1 K_2 + K_3) + a^2 K_1 K_3 \qquad \text{(B-12)}$$

$$K_h = (K_1 K_2 + K_3 - aK_1 K_3)/K_\gamma \qquad \text{(B-13)}$$

$$K_I = K_1 K_3 / K_\gamma \qquad \text{(B-14)}$$

Note that "a" from (B-7) is updated continuously during a trajectory and represents a compensation term to account for $\dot{E}$ dynamics. Setting a = 0 reduces the solution to the form illustrated in Figure B-1.

REFERENCES

[1] Calise, A.J., "Interim Report - A Singular Perturbation Analysis of Minimum Time Long Range Intercept", 7 July, 1978.

[2] Calise, A.J., Moerder, D.D., "A Singular Perturbation Analysis of Minimum Time Long Range Intercept", Final Report for the period 1 February - 31 December, 1978.

[3] Calise, A.J., Moerder, D.D., "A Singular Perturbation Analysis of Minimum Time Long Range Intercept", Semi Annual Progress Report, January - June, 1979.

[4] Calise, A.J., "Singular Perturbation Techniques for On-Line Optimal Flight Path Control," AIAA Atmospheric and Flight Mechanics Conference, Paper No. 79-1620, Boulder, Colorado, August 6-8, 1979.